

Review

Exploring the Biosorption of Methylene Blue Dye onto Agricultural Products: A Critical Review

Manish Kumar Sah¹, Khaled Edbey², Ashraf EL-Hashani³, Sanad Almshty³, Luisetto Mauro⁴, Taghrid S. Alomar^{5,*} , Najla AlMasoud^{5,*}  and Ajaya Bhattarai^{1,*} 

¹ Department of Chemistry, Mahendra Morang Adarsh Multiple Campus, Tribhuvan University, Biratnagar 56613, Nepal

² Libyan Authority for Scientific Research, Tripoli P.O. Box 80045, Libya

³ Department of Chemistry, University of Benghazi, Benghazi P.O. Box 1308, Libya

⁴ Pharmaceutical Department PC AREA, Applied Pharmacologist, 29121 Piacenza, Italy

⁵ Department of Chemistry, College of Science, Princess Nourah bint Abdulrahman University, Riyadh 11671, Saudi Arabia

* Correspondence: tsalomar@pnu.edu.sa (T.S.A.); nsalmasoud@pnu.edu.sa (N.A.); bkajaya@yahoo.com or ajaya.bhattarai@mmamc.tu.edu.np (A.B.); Tel.: +977-9842-077-434 (A.B.)

Abstract: Due to their higher specific area and, in most cases, higher adsorption capacity, nanomaterials are noteworthy and attractive adsorbents. Agricultural products that are locally available are the best option for removing methylene blue (MB) dye from aqueous solutions. Because it is self-anionic, FT-IR and SEM investigations of biosorption have confirmed the role of the functional group and its contribution to the formation of pores that bind cationic dye. It is endothermic if the adsorption of MB by an adsorbent is high as the temperature increases; on the other hand, exothermic if it is high as the temperature decreases. A basic medium facilitates adsorption with respect to pH; adsorption is proportional to the initial concentration at a certain level before equilibrium; after equilibrium, adsorption decreases. A pseudo-second-order model applies for certain agricultural products. As per plotted graph for the solid-phase concentration against the liquid-phase concentration, the Langmuir adsorption isotherm model is favored; this model describes a situation in which a number of molecules are adsorbed by an equal number of available surface sites, and there is no interaction between adsorbate molecules once all sites are occupied. In contrast, the Freundlich model depicts non-ideal multi-layer sorption onto heterogeneous surfaces via numerical analysis; with a value of $n = 1$, the result is a linear isotherm. If the value of $n < 1$ or $n > 1$, then it is chemical or physical adsorption, respectively. Based on an EDX analysis, relevant elements are confirmed. BET analysis confirms the surface area. Nanoproducts categorized as agricultural products exhibit the aforementioned tendency. Even though nanoparticles show positive outcomes in terms of higher adsorption, a high specific area for the targeted pollutant is needed in real-world applications. In the relevant sections herein, the behavior of thermodynamic parameters, such as enthalpy, entropy, and Gibbs free energy, are examined. There is some question as to which form of agricultural waste is the most effective adsorption medium. There is no direct answer because every form of agricultural waste has its own distinct chemical and physical characteristics, such as porosity, surface area, and strength.

Keywords: biosorption; methylene blue; SEM; agricultural product; enthalpy; entropy; temperature



Citation: Sah, M.K.; Edbey, K.; EL-Hashani, A.; Almshty, S.; Mauro, L.; Alomar, T.S.; AlMasoud, N.; Bhattarai, A. Exploring the Biosorption of Methylene Blue Dye onto Agricultural Products: A Critical Review. *Separations* **2022**, *9*, 256. <https://doi.org/10.3390/separations9090256>

Academic Editors: Yu-Chie Chen and Karuppachamy Selvaprakash

Received: 23 July 2022

Accepted: 31 August 2022

Published: 13 September 2022

Publisher's Note: MDPI stays neutral with regard to jurisdictional claims in published maps and institutional affiliations.



Copyright: © 2022 by the authors. Licensee MDPI, Basel, Switzerland. This article is an open access article distributed under the terms and conditions of the Creative Commons Attribution (CC BY) license (<https://creativecommons.org/licenses/by/4.0/>).

1. Introduction

There are many industrial applications of synthetic dyes, which include carpets, leather, paper, printing, food, cosmetics, petroleum, rubber, plastic, and photography [1].

Due to the industrial waste from these industries, light penetration can be reduced [2]. Many dyes have been classified as carcinogenic and toxic because they have negative effects

on human health and the environment [3,4]. MB dye (its chemical name is tetramethylthionine chloride) is also known as methylthioninium chloride and has a significant blue color in its oxidized form; it is colorless in its reduced form [5], as shown in Figure 1.

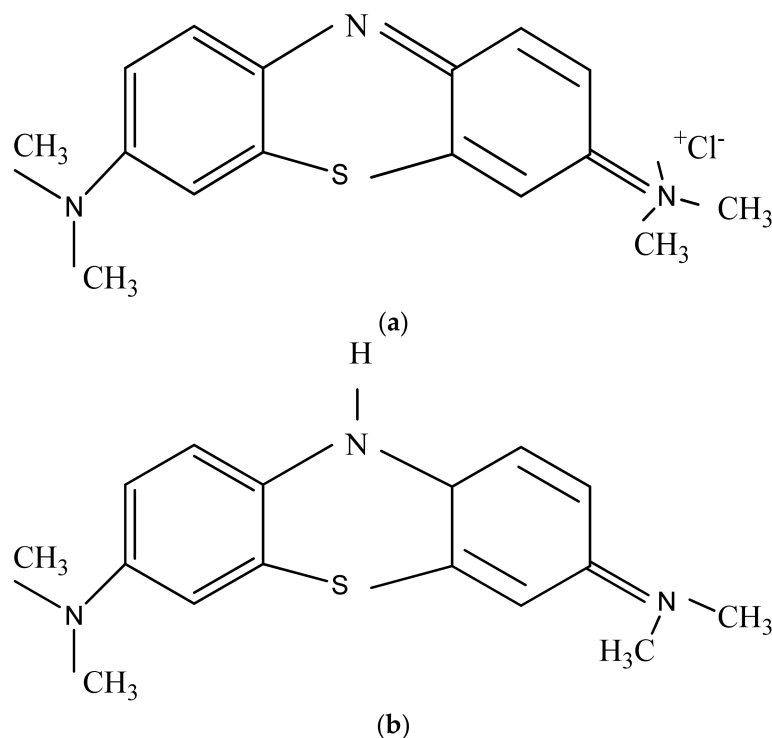


Figure 1. (a) MB (blue); (b) Leukomethylene blue (colorless).

MB dyes have multiple uses and are classified as very important basic dyes. The presence of aromatic amines in the dye makes it very harmful to humans [6]. When a human is exposed to methylene blue, symptoms such as high heart rate, vomiting, and tissue myonecrosis appear [7]. Hence, the elimination of this dye from aqueous solutions is necessary. Many techniques have been used to remove dyes from industrial waste, including biological treatment, adsorption, membrane technologies, ozonation, flocculation, physicochemical methods, chemical precipitation, ion-pair extraction, and photolysis [8]. Recently, there has been increased interest in the use of plant waste (agricultural products) for dye removal; these products can be used for dye adsorption from aqueous solutions because of their natural availability and high levels of removal efficiency. Such materials are easily and locally available in developing and under-developed countries. The biosorption behavior of agricultural products is defined as the ability of a surface to adsorb dye by utilizing agriculturally based materials.

In general, biosorption is defined as the process of binding contaminants within the cellular structures of a biomass. A metabolically mediated path to heavy metal accumulation can be achieved using this process [9].

The advantages of agro-waste as an adsorbent for removing MB from water are its low cost, energy efficiency, accelerated kinetics, maximum carbon content, and regenerative properties. From a socio-economic perspective, agricultural waste is inexpensive, and when waste is converted into an effective adsorbing reagent, agricultural waste expenditures are eliminated, and the adsorbing agent offers opportunities for commercialization.

On the other hand, several disadvantages have been observed. For example, NaOH, KOH, and ZnCl₂ are required to improve the porous structure of the adsorbent. Under natural conditions, not all agricultural waste can provide the most efficient adsorption. It is often necessary to use chemicals to adjust pH and porous structure [10]. Additionally, the removed dye can cause further environmental problems that must be managed, and the

same adsorbent may not be used for the adsorption of other dyes, which does not appear to be a holistic approach.

As local resources are used, the cost is also low in comparison to synthetic products. The relevant research is lab-based, not applied research. If this solution is to be implemented on an industrial scale, then cost analysis is also important. Herein, the removal of MB by agro-waste in the literature published between 2011 and 2021 is discussed. The removal of MB by agro-wastes such as rice husk [11,12], modified wheat husk [13], the sawdust of various trees [14–16], the peels of fruits [17], seeds [18,19], and the leaves of various plants [20–23] has been studied. For the removal of MB from aqueous solutions, sugarcane bagasse is an excellent and relatively low-cost adsorbent [24]. MB dye is soluble in sugarcane bagasse treated with acid [25]. Using groundnut shell powder as a fixed bed, MB can be removed from aqueous effluent [26]. In wastewater treatment, organosolv lignin (OL) is a promising adsorbent, owing to its high phenolic and aliphatic hydroxyl content. OL was extracted from steam-exploded rice straw using mixed solvents and used as a byproduct to remove MB in the study described in [27].

As a result of the harvest of olive fruits, tons of olive tree pruning waste (OTPW) are set on fire in the fields, polluting the atmosphere with greenhouse gases. OTPW management is, therefore, of critical environmental importance in areas that produce olive oil. Olive tree pruning waste biomass is effective at removing MB from aqueous solutions, with an efficiency of 129.87 for OTPW [28].

Many agricultural solid wastes are used for the removal of dyes from aqueous solutions. *Ficus carica* is a species of flowering plant in the mulberry family, known as the common fig. *Ficus carica* bast activated carbon (FCBAC) can be used to remove methylene blue [29]. A review article focused on determining the contact time, initial dye concentration, dosage of adsorbent, and pH of the MB solution. The Langmuir, Freundlich, and Temkin isotherm models were tested. There are also studies that examine MB adsorption using raw pinecone biomass (*Pinus radiata*) [30].

By means of batch adsorption, tobacco (*Nicotiana tabacum* L.) stem ash (TSA) was demonstrated to be a suitable adsorbent for the removal of MB from water [31]. MB may also be removed using pine sawdust modified with citric acid (CA-PS) [32]. However, it is also utilized to remove MB from single and binary systems [33]. The kinetics, equilibrium, and thermodynamic properties of carbon synthesized from plant leaf powder were studied for the adsorption of MB [20]. Another potential resource for MB removal is the rice sugar extracted from spent biomass [34]. MB was removed from biomass using *Arthrospira platensis* in [35]. In the literature, MB was also detected in raw and pretreated *Spirogyra* sp. [36]. Using brown macroalga, Daneshvar et al. studied MB dye desorption [37].

In 2006, Nacèra and Aicha performed equilibrium and kinetic modeling of MB biosorption on dead streptomyces rimosus that had previously been pretreated [38]. Equilibrium and thermodynamics of MB adsorption on Ephedra strobilacea sawdust were explored by Agarwal et al. They also looked at the effects of phosphoric acid and zinc chloride modifications on kinetics, equilibrium, and thermodynamics [39].

A study published in 2013 [40] reported the adsorption of MB by sugarcane bagasse modified with EDTA dianhydride (EDTAD) in aqueous solutions. As a consequence, Nasuha and Hameed observed MB adsorption from an aqueous solution on NaOH-modified rejected tea [41].

In the literature, chemically modified cellulose waste was found to be a biosorbent with respect to MB [42]. Using ground raw and base-modified pinecone powder, Yagub et al. removed the cationic dye MB from an aqueous solution in 2013 [43]. In another study, Spagnoli et al. examined methylene blue's adsorption on activated cashew nutshell carbon [44].

MB was removed from aqueous solutions using natural and carbonized Brazilian pine-fruit shells as adsorbents [45]. Yellow passion fruit waste was used by Pavan et al. to study MB biosorption [46]. Water hyacinth compost was utilized to study biosorption; efficient microorganisms were used to create this compost and to use biosorption to get rid

of basic dyes [47]. An evaluation of the red marine alga *Alga Kappaphycus alvarezii* as a biosorbent for MB biosorption was reported in [48]. A study of the biosorption of MB onto *Gracilaria corticata*, a red seaweed, can be found in [49]. A 2011 article [50] by Kumar et al. indicated that agricultural wastes could desorb dye from aqueous solutions. In another study, peanut husk allowed for MB adsorption in batch and column modes [51].

Therefore, the sorption technique has been proven to be an adequate method for the reuse of water [52]. It is a simple and easy operation with very low costs.

There is also some literature on the adsorption of MB dye using the plant waste of castor plants. For example, a castor seed shell was used to remove MB in [53].

In addition, four major functional groups in the matrix of castor seeds (amines, carboxyls, azos, and hydroxyls) were studied for their roles in MB adsorption [18].

Figure 2 illustrates the large, umbrella-like, palmately arranged leaves of the castor plant [54].

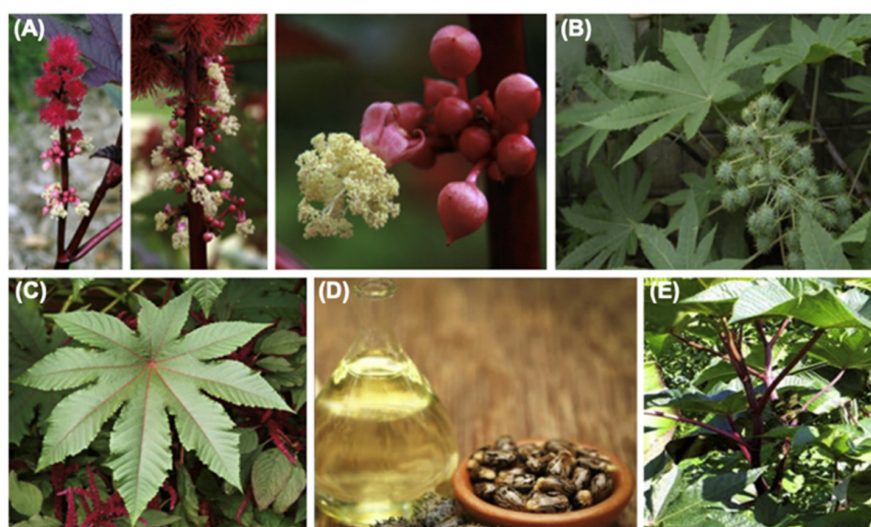


Figure 2. Castor plant (A) flower, (B) seed, (C) leaf, (D) seed and oil, and (E) stem (adapted from [54]).

Specifically, the leaf and stem of the castor plant contain the most lignocellulosic material. Castor leaves contain 57.4 g of carbohydrate, 24.8 g of protein, 10.3 g of fiber, 5.4 g of fat, 12.4 g of ash, 2670 mg of calcium, and 460 mg of phosphorus per 100 g. Epicatechin and isoquercetin are contained in the leaves of the castor plant [55].

Castor plant fibers are composed of cellulose fibers, which are the main component of castor paper. Sugarcane bagasse can be used by the paper and pulp industry as a raw material to make paper. The residues of castor, if used in the paper and pulp industry, would increase the earnings of castor-growing farmers and provide raw material to an industry that is otherwise dependent on forest, agro-forestry, and agro-based byproducts for its raw materials [56]. GCH-7 castor stem contains 45.7% cellulose and 17.2% lignin. Therefore, it could be concluded that castor, which is the only natural source of ricinoleic acid, may be explored as a potential raw material for paper industries due to its high cellulose and low lignin content.

2. UV-VIS Spectrophotometer

A UV-VIS spectrophotometer was used to determine the concentration of MB dye in solution in [57]. The UV-VIS absorption spectra of MB were recorded by Wang et al. [58] in the range of 200–800 nm, as shown in Figure 3. In the UV region, MB showed two intense absorption bands that registered between 245 and 295 nm; the same result was also observed by Sachin et al. [59]. Ahmed et al. [60] also noted that MB displayed one strong absorption band between 650 and 700 nm in the visible area.

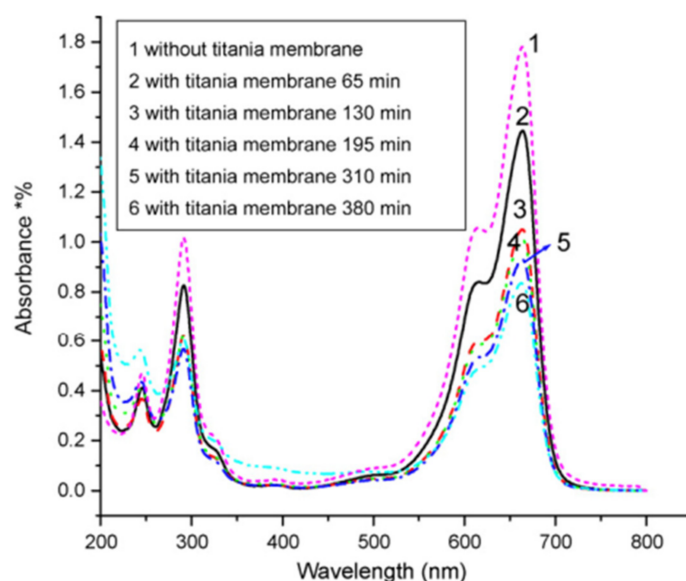


Figure 3. UV-VIS absorption spectra of MB with and without titania membrane (MB spectrum 1 without titania membrane, pink color) in the range of 200–800 nm [58].

3. Langmuir Sorption Ability

The maximum MB adsorption values (Q_m (mg/g)) obtained for various sorbents are listed in Table 1.

Table 1. Langmuir sorption ability (Q_m in mg/g) of various sorbents of MB.

Sorbent	Q_m (mg/g)	Reference
Castor seed shell	158.73	[53]
Oxalic-acid-modified rice husk	53.21 ± 2.43 (293 K)	[10]
	66.90 ± 3.44 (303 K)	
	70.10 ± 3.43 (313 K)	
Natural rice husk	19.77 ± 1.83 (293 K)	[10]
Magnetic alginate/rice husk	274.9	[11]
Modified wheat husk	4.23 (303 K)	[13]
	4.04 (313 K)	
	3.78 (323 K)	
<i>Posidonia oceanica</i> (L.) dead leaves	217.39 (298 K)	[23]
	270.27 (308 K)	
	285.71 (318 K)	
Rice husk activated carbon	9.83 (303 K)	[12]
	10.62 (313 K)	
	14.34 (323 K)	
Flamboyant pods activated carbon	874.68	[19]
Sugarcane bagasse	108.69	[24]
Groundnut shell powder	242	[26]
Organosolv lignin from rice straw	40.02	[27]
Acid-treated sugarcane bagasse	64.9351	[25]
Olive tree pruning waste	129.87 (298 K)	[28]
Compost of olive tree pruning waste	250.00 (298 K)	[28]
<i>Arthrospira platensis</i> (cyanobacterium)	312.50 (298 K)	[35]
Raw <i>Spirogyra</i> sp. (green alga)	50.70 (293 K)	[36]

Table 1. Cont.

Sorbent	Q _m (mg/g)	Reference
Pretreated <i>Spirogyra</i> sp. (green alga)	64.61 (293 K)	[36]
<i>Nizamuddinina zanardini</i> (brown macroalga)	95.45 (300 K)	[37]
Pretreated dead <i>Streptomyces rimosus</i>	34.34 (293 K)	[38]
<i>Ephedra strobilacea</i> char	31.055(298K)	[39]
<i>Ephedra strobilacea</i> char modified using phosphoric acid	21.881 (298 K)	[39]
<i>Ephedra strobilacea</i> char modified using ZnCl ₂	37.174 (298 K)	[39]
Sugarcane bagasse modified with EDTA dianhydride (EDTAD)	202.43 (298 K)	[40]
NaOH-modified rice husk	39.2 ± 2.7 (298 K)	[40]
NaOH-modified rejected tea	242.11 (303 K)	[41]
Cellulose waste modified with citric acid	211.42 (293 K)	[42]
Raw pinecone	129.87 (303 K)	[43]
Pinecone modified with 0.1 M NaOH	142.86 (303 K)	[43]
Pinecone modified with 0.05 M NaOH	135.13 (303 K)	[43]
Carbon derived from cashew nut shell activated with ZnCl ₂	456	[44]
Pine-fruit shell (<i>Araucaria angustifolia</i>)	185 (298 K)	[45]
Yellow passion fruit	44.70 (298 K)	[46]
Effective microorganism (EM)-based water hyacinth compost	295.65	[47]
Red marine (<i>alga Kappaphycus alvarezii</i>)	74.40 (303 K)	[48]
<i>Gracilaria corticata</i> (red seaweed)	95.41(303K)	[49]
(<i>Ficus carica</i> bast) FCBAC	47.62	[29]
<i>Pinus radiata</i> cone	109.89	[30]
Tobacco stem ash	35.7(300K)	[31]
Modified sawdust	111.46 (293 K)	[32]
	114.40 (303 K)	
	156.6 (313 K)	
Carbonized plant leaf powder from teak (<i>Tectona grandis</i>) and guava (<i>Psidium guajava</i>) trees	61.22	[20]
Sugar extracted from spent rice biomass	8.30	[34]
Cashew nut shell	5.31	[50]
Peanut husk	72.13 ± 3.03	[51]
Biogenic zirconium oxide (ZrO ₂)	23.26	[61]
Fe ₃ O ₄ magnetic nanoparticles	1374.6	[62]
Nano-silica (nSiO ₂)	679.9	[63]
Fe-Mn binary oxide	72.32	[64]

4. Fourier Transform Infrared (FT-IR) Spectroscopy

Functional groups are found using the Fourier transform infrared (FT-IR) spectroscopy technique. This technique was applied in this review article to analyze the nature of materials before and after MB adsorption. A diverse curve reflects varied composition; in such cases, analysis must be conducted by the researcher, including a collective analysis of the cationic and anionic nature of the material with respect to stabilization and impact on

MB dye adsorption. Generally, agricultural product waste contains cellulose, hemicellulose, and lignin. The relevant functional groups have been identified, and there is diversification within the category; notable examples are given in Table 2.

Table 2. The functional groups of varieties of agricultural waste containing cellulose.

Presence	cm ⁻¹	Reference
OH groups associated with silanol groups (Si-OH) to adsorb water	3300–3450	[25]
OH groups bound to methyl radicals observed in lignin structures	2920–2940	[18,26,29,40,41]
Peaks showing carbonyl stretching from aldehydes and ketones	1640–1670	[32,33]
Peaks showing aromatic rings	1511	[14,32,40]
Structures of SiO ₂ , i.e., silica	1130–1050	[25]
Bending vibration of SiO ₂	466	[25]
Asymmetric stretching of -COO- group vibrations	1592	[40]
Symmetric stretching of -COO- group vibrations	1412	[40]
Peaks showing asymmetric and symmetric stretching of -CH ₂ groups	2914	[30]
Peaks showing symmetric stretching of -CH ₂	2868	[30]
Peaks showing vibration stretching of CO	1076	[32,33]
The peak of ester acetyl groups in carboxylic acid groups of lignin or hemicellulose	1700	[14,40]
Stretching vibration of Si-O bond in rice husk structure	800	[2,11,14,41]
Stretching vibration of -C=N	1594	[11,14]
Stretching vibration of -C-N	1334	[11,14,36]
Stretching vibration of -C=S	1492	[11]

According to an experiment performed on natural rice husk (NRH) and modified rice husk (MRH), these materials can be used for the adsorption of aqueous solutions of MB. Of importance is the number of carboxyl groups (MRH > NRH) that serve as proton donors. Hence, deprotonated OH and carboxyl groups coordinate with positive dye ions. The positively charged ion species, i.e., MB and MG, influence the attraction of anionic MRH structures, which shows the high adsorption ability of MRH with respect to MB [10].

Similarly, an experiment was performed in which magnetic alginate/rice husk (m-ALG/RH) bio-composite beads were synthesized by depositing rice husk into an alginate solution; this increased the synergistic effect that enables adsorption. Due to the H-bonding interaction of MB molecules and m-ALG/RH bio-composite beads, wide peaks shifted from 3200 cm⁻¹ to 3400 cm⁻¹ after MB adsorption; this indicates MB adsorption. The above-mentioned (-C=N, -C-N, and C=S) peaks of stretching represent vibrations in the dye molecules [11].

In addition, carbonization changes the chemical nature of cellulosic material, such as rice husks, and forms activated carbon, which plays a vital role in the adsorption of MB [12]. Alcohols, esters, and carboxylic acids are present in the molecular structures of the major components of natural white pine sawdust (NS). There is a carboxy group present in hemicellulose, but it is a minor component in NS. The band observed at 2916 cm⁻¹ corresponds to the C-H group, owing to cellulose, hemicellulose, and lignin. Lastly, the band at 3324 cm⁻¹ is due to the O-H groups, mostly present in cellulose. When NS is mixed with MB, two strong bands are observed, i.e., -C=N- stretching in the poly-heterocycles and -C-N- stretching in the amine groups, along with one weak band (-C-H out-of-plane bending in the aromatic rings), all of which is behavior associated with MB [14]. This accords with an analysis by V. Dharmalingam et al., who examined the behavior of four major functional groups within the biomass of castor seeds with respect to the adsorption of seven dyes. Said study examined the dye adsorption mechanisms of castor seeds. Methylation reduced the broad mixed stretching vibration adsorption band of the amino

and hydroxyl groups. Esterification reduced the stretching vibration adsorption band of the carboxy bond. The stretching vibration adsorption band of the carboxyl group increased due to the acetylation of the amino and hydroxyl groups [18]. In addition, both untreated and acid-treated sugarcane bagasse are composed of many functional groups that form active sites for the adsorption of methylene blue. As a result, one could observe the percentage transmittance of the biomass, the shifting or disappearance of the bands at 2920, 1260, 1040, and 500–400 cm^{-1} , and the appearance of new bands at 1200, 1060, and 880–840 cm^{-1} .

The peaks refer to -OH/N-H, -C=O, C-OH, SiO_2 , and the C-halogen bonds on the surface of the biomass used in the sorption process [25].

MB, a cationic dye, was removed from groundnut shells using shell powder, which is a waste product after oil production; -OH is present on the surface of groundnut shell powder (GNSP), which increases the interaction between adsorbent and adsorbate and, consequently, the adsorption of MB [26]. A similar result was obtained when activated carbon developed from *Ficus carica* bast was applied for the adsorption of MB; the broad absorption peak of the O-H stretching vibration showed the presence of alcohols, phenols, and carboxylic acids, as found in pectin, cellulose, and lignin, available as “free” hydroxyl groups on the adsorbent surface. When dye was adsorbed on the functional groups of activated carbon (FCBAC), additional peaks of N, O, C-N, >C, O, and C-S were observed; this reflects the interaction of the dye molecules with the functional groups of the biosorbent [29].

Pinecone biomass (*Pinus radiata*) formed by the pine tree also contains an -OH group on the surface that shows the presence of cellulose, hemicellulose, lignin, rosin, and tannins in the cell walls; these have polar functional groups, such as alcohols, aldehydes, ketones, carboxylic compounds, and phenolic compounds. It is interesting to observe the vibration of CH_n , especially due to -CH and - CH_2 bonds at 2926.87 cm^{-1} , as described in the literature [30]. The modified form of sawdust increased the absorption band for the stretch vibration of the carboxyl group at 1735 cm^{-1} .

Citric-acid-modified sawdust (CAMS) has more carboxyl groups than raw sawdust and displays high physical and surface activity. The intensity of the group bands (CO and >C=O) shows the maximum C-O available in the adsorbent; it acts as a proton donor, due to which the deprotonated hydroxy and carboxyl groups coordinate with positive dye ions. In addition, positively charged MB ions are attracted toward the anionic CAMS structure. Hence, CAMS shows a strong adsorption capacity with respect to MB ions. Many functional groups were detected after adsorption, even though some peaks were shifted or disappeared; the functional groups of CMAS were detected at bands of 1598, 1331, and 883 cm^{-1} , which indicated the bonded C=O groups, aromatic nitro compounds, and C-C groups. This result shows the functional groups present on the surface of CAMS during the MB adsorption process [32].

FT-IR shows the presence of C-H, OH, and >OC in the cellulose of pine sawdust, as is generally the case (PS). The major differences observed between NaOH-treated pine sawdust (B-PS) and pine sawdust modified with citric acid (CA-PS) consist of stretching vibration adsorption bands at 1740 cm^{-1} (>CO) and 1425 (>CO coupled with delta OH) cm^{-1} ; this shows the increment in the COOH group via esterification. The surface of CA-PS is characterized by the carboxyl group. Due to its porous structure and irregular surfaces, many free carboxyl groups are introduced; this resembles the process by which esterification changes the surface chemistry of B-PS, and allows citric-acid-modified PS to maximize its capacity to adsorb. It can be concluded that esterification changes the surface chemistry of B-PS, and citric-acid-modified PS has adequate physical and chemical characteristics to adsorb MB ions within a single frame [33]. In another example [34], inter- and intra-molecular -OH on the surface of spent rice biomass (SRB) have a similar effect on MB [26,29]. When raw and pretreated *Spirogyra* sp. are applied for the single and binary biosorption of MB, FT-IR reveals carboxyl, amino/hydroxyl, carbonyl, carboxylic, and phenolic groups that are present on the cell walls of *Spirogyra* sp.

The peak at 524 cm^{-1} represents C-N-S, due to the polypeptide structure. A decrement in the absorption peak is noted due to the interaction of ionized functional groups (carboxyl, amino, amide, and hydroxyl groups) with protons or metal ions; in addition, MB is a cationic dye. Moreover, all other peaks of pretreated *Spirogyra* sp. are similar to those of other plants or biomass [36].

Note the presence of both the surface hydroxyl (-OH) stretching of the carboxylic groups and the stretching of the amido groups (-NH). The other peaks were observed at 1637.12 and 1034.70 cm^{-1} , i.e., -C=C and aromatic ethers and aryl-O stretching. The -OH on the surface served as the binding agent for MB dye [37]. The FT-IR spectrum of EB showed the appearance of strong bands at 1743 cm^{-1} , 1631 cm^{-1} , and 1406 cm^{-1} ; these results show the asymmetric and symmetric axial deformations of carboxylate (-COO-), which is confirmatory for the introduction of EDTA dianhydride due to the formation of ester linkages and the release of carboxylate functions that bind MB dyes into the lignocellulose matrix [40].

Distinct behavior was noticed for raw rejected tea (R-RT) and NaOH-modified rejected tea (N-RT). The two new peaks at 2919 and 1427 corresponded to aliphatic C-H and NH_2 deformations. After adsorption, the shifting of -OH, C=O, and -C- was noted, which reflected the binding of MB at -OH and C=O. The physical stability of N-RT is greater than that of R-RT, which can be observed in the fact that more functional groups were observed in the analysis of N-RT [41].

All the products discussed herein belong to agro-species that contain cellulose, hemicellulose, and lignin; these materials include rice husk, rejected tea, pine sawdust, etc. [2,14,41]. It is well known from the literature that cellulose contains N-H bonding, as well as -C=O and -OH groups. The observed peaks and broad peaks only differed due to deprotonated OH and carboxyl groups coordinating with positive dye ions. On the other hand, methylation also played a role in reducing the broad mixed stretching vibration adsorption band of the amino and hydroxyl groups [18]. The carboxyl group also acted as a proton donor that formed the anionic structure of the materials. Hence, the anionic formation that occurred due to -OH and -C=O compounds resulted from their role serving as proton donors and being anionic, which attracted MB species.

5. SEM

To ascertain the morphology and acquire imaging of the microstructures, scanning electron microscopy (SEM) investigation was used. This method can be used to comprehend the behavior and morphology of agricultural items both before and after the dye has been absorbed. When hen feathers (waste materials) were used for adsorbing MB dye, the SEM micrograph reflected a maximum surface area that was sufficient to trap MB on its surface via functional groups, as shown in Figure 4 [1]. The surface morphologies of m-ALG, magnetic alginate/rice husk (m-ALG/RH), and MB adsorbed onto m-ALG/RH bio-composite beads were analyzed by SEM; results reflected the fact that the roughness and morphological regularity of the surface of the m-ALG beads increased via the rice husk's incorporation into the magnetic biopolymer.

MB molecules were conglomerated within the layers of the bio-composite surface after adsorption, which is sufficient for the action of adsorption [11]. The presence of pores and the internal surface were imaged via SEM before adsorption; the image taken after the adsorption of MB makes it appear that the porous structure was blurred via adsorption. The particle size distribution was $0.213\text{ m}^2/\text{gm}$ with reference to the average surface weight. The size of pinecone biomass was $28.19\text{ }\mu\text{m}$ when *Pinus radiata* was applied for the removal of MB dye, as shown in Figure 5 [30].

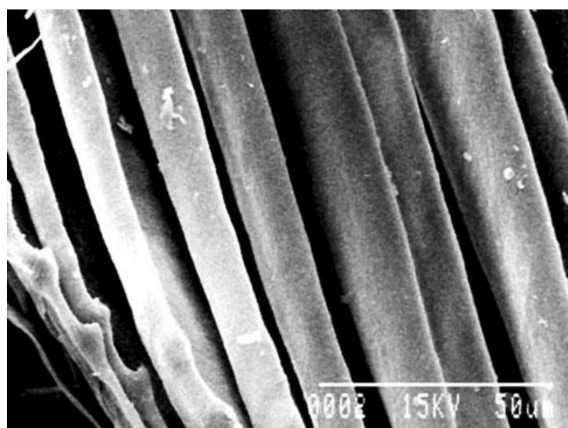


Figure 4. SEM micrograph of HF (magnification: 10,009) [1].

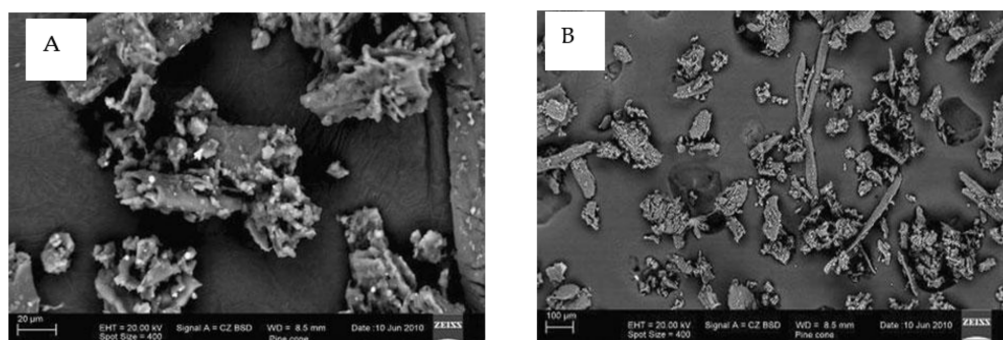


Figure 5. (A) SEM image of pinecone biomass before adsorption. (B) SEM image of pinecone biomass after MB adsorption [30].

SEM imaging observed small pits within the surface layers of cellulose after rice husk activated carbon was used for MB adsorption, which reflects the number of pores by which MB was trapped and adsorbed [12]. An SEM image of modified wheat husk (MWH) shows the amorphous behavior of the modified wheat husk.

The image illustrates maximum roughness; the presence of many lumps on the surface of the adsorbent suggests that the adsorbent is an excellent material for the adsorption of dyes, as seen in Figure 6 [13]. In another example, the differences in images captured before and after the adsorption of MB show MB on activated carbon prepared under optimized conditions (ACop), where ACop involves the preparation of the activated carbon via flamboyant pod (*Delonix regia*) dyes with a $ZnCl_2$ activating agent [19]. Similarly, examination of an SEM micrograph of *Ficus carica* activated carbon (FCBAC) reveals its porous nature, which presents adequate space for MB adsorption [29]. The surface of natural sawdust (NS) is too smooth, with vertical grooves, compared to citric-acid-modified sawdust (CAMS), which is able to adsorb dye due to its irregularity.

Thus, the adsorption of an adsorbate is possible using a different part of CAMS [32]. Micrographs of the adsorbent surface both before and after the adsorption of MB dye reflect monolayer adsorption on the surface of spent rice biomass (SRB). This also supports the Langmuir biosorption isotherm model [34].

As per SEM images, *Spirogyra* sp. algae cells have a complex, intricate, uneven, and irregular surface with a filamentary structure. After exposure to MB, the gaps of the surface became filled with dye molecules [36]. Relatedly, an SEM image shows that *N. zanardinii* has a very high number of granules on its rough surface.

Such nano-granules maximize surface area and the surface-to-volume ratio, thereby creating a large surface area for MB sorption due to the granular surface of algae. Moreover, several pores have been observed. There are also tiny particles that are directly proportional to sorption capacity [37]. SEM micrographs of N-RT before and after MB adsorption reflect

the increase in pores of the macro reticular type on the surface of N-RT. For example, see the honeycomb-shaped gaps observable after modification with NaOH solution and the associated enhancement of the physical features, as visible in Figure 7 [41].

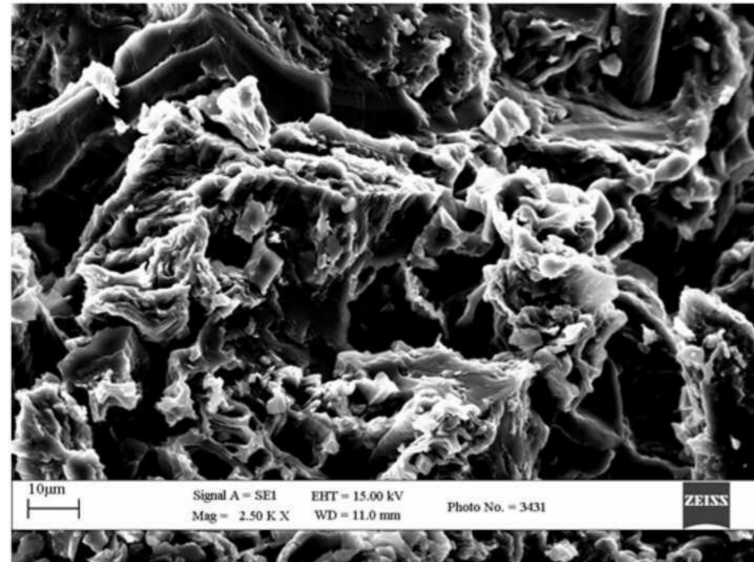


Figure 6. SEM image of modified wheat husk [13].

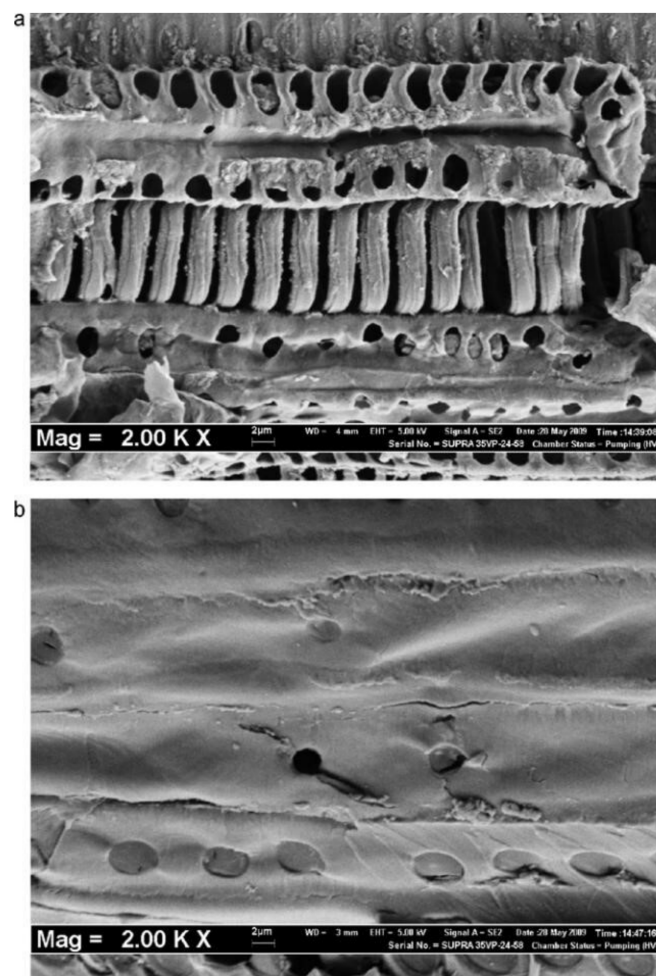


Figure 7. (a) NaOH-modified rejected tea (N-RT) before dye adsorption and (b) NaOH-modified rejected tea (N-RT) after dye adsorption [41].

The porous internal surface structure visible before the adsorption was covered up after adsorption; this change reflects the presence of MB mixed with ground raw and base modified pinecone powder [43]. The SEM image suggested that the control, EM_{WHC}, was rough; it had a large number of pores that increased the surface area for the bonding of dyes. It was confirmed that the pores were occupied by MB dye molecules [47]. The differences observed before and after the adsorption of MB showed a porous morphology that was analyzed by means of variation in the composition of the soft segments of the polymers. Observations of porousness might have been due to the increase in -OH and -CO groups; they support the binding and interaction of MB dye and ascorbic acid molecules when the green synthesis of biodegradable polyurethane and a castor-oil-based composite is applied [65].

The SEM analysis also showed the morphology of a solid structure where mangosteen peel activated carbon (MPAC) had a large specific surface area of porous features that was distinct from other forms of activated carbon created from corn cobs or grape seeds; the nature of the morphology reflected the binding behavior of MB [66]. As mentioned above, the pores and vacant spaces that are available in various agricultural products adsorb MB dye by providing a pathway for the bonding of dyes. An SEM can scan the surface properties of materials, whereas FT-IR analyses of such materials reflect the presence of -OH on the surface of the materials. The presence of certain functional groups, such as -OH, >CO, -CO, etc., plays a vital role in the porous nature of such materials.

These findings are also cited in the literature [65]. The surface area and the number of pores are directly proportional to the number of functional groups, and they increase the rate of sorption capacity.

6. Thermodynamic Analysis

In order to determine the spontaneity, endothermic or exothermic behavior, and randomness of the molecules, respectively, calculations of the Gibbs free energy (GFE), enthalpy (H), and entropy (S) are used in thermodynamic analysis. For example, when CAMS was used for adsorption, the negative value of ΔG represented the spontaneity behavior of adsorption at a given temperature. Moreover, the adsorption of MB onto CAMS was excellent at higher temperatures, where the negative value of ΔG was in the decrement phase as temperature increased due to the enlargement of pore size. Such pores were active sites of CAMS that were reused for the adsorption of MB at least three times; this can be confirmed via the random nature of adsorption [32]. When modified pinecone powder was applied for the removal of MB, it resulted in spontaneity ($-\Delta G$) behavior of adsorption at a given temperature. Pinecones were favorable for the adsorption of MB at lower temperatures as there was an increment in the positive value of ΔG , whereas sorption was exothermic as ΔH was negative. The $-\Delta S$ indicated a decrement in the randomness behavior of the solid-solute interface [43]. A similar observation applied for spontaneity, i.e., there was a negative value of ΔG for the physical adsorption of MB on biomass. A positive value of ΔG increased along with increases in temperature, which showed that adsorption was favored at a lower temperature, whereas a negative value of ΔS reflected a decrease in the randomness of the solid-liquid interface. On the other hand, $-\Delta H$ represented adsorption with an exothermic nature [30]. A negative value of ΔG for temperatures 25–50 °C represented the spontaneity behavior of the biosorption. A positive value of ΔH reflected the endothermic behavior of the biosorption process, which can be analyzed via the removal of the higher dye concentration from the aqueous phase (>45 mg/L) at 45 °C. The value of ΔS showed an increment in randomness at the dye-SRB interface and led to a high quantity of dye removal [34]. A similar observation was also evident during the use of FABAC for MB dye, i.e., adsorption in this case was an endothermic process, meaning that there was a positive value of ΔH .

A positive value of ΔS represented an increment in the randomness behavior of adsorption [29]. Adsorption was also endothermic in nature in this case, and the rate of spontaneity was also high; as a result, dye could remove water molecules from the

adsorbent, and dye adhered to the surface of the adsorbent when NaOH-modified rejected tea was applied for the adsorption of MB dye [41]. Similarly, when carbonized plant leaf powder was applied for the adsorption of MB, the spontaneity of the reaction was reflected by a negative value of ΔG , and the reaction was endothermic in nature (ΔH), whereas there was an increment in randomness with a positive value of ΔS for the dye molecules on the solid surface after adsorption. The quantity of dye uptake was directly proportional to the increment in temperature [20].

Differences were also visible when the material used was raw *Spirogyra* sp.; pretreated *Spirogyra* sp. showed different thermodynamic behavior. The spontaneity was characterized by a negative value of ΔG during the biosorption of MB. The value of ΔH was negative for both raw and pretreated *Spirogyra* sp. Such behavior showed the exothermic nature of MB adsorption in this case. The positive value of ΔS reflected the randomized nature of the solid–liquid interface of biosorption [36]. There were interesting facts observed during the application of olive tree pruning waste (OTPW) and composted olive tree pruning waste (COTPW) with respect to the spontaneity and exothermic behavior of the reaction. On the other hand, the data for OTPW and COTPW resulted in positive values and negative values, respectively, of ΔS ; this shows an increment and a decrement, respectively, in the randomness during biosorption [28]. All the thermodynamic parameters were observed within the solid–liquid interface, which shows the activation sites on the surface that bind dye. See also [39].

A positive value of ΔS corresponds to an increase in randomness, and a negative value of ΔG indicates the spontaneous behavior of adsorption. A negative value of ΔH corresponds to an exothermic reaction, and a positive value of ΔH indicates an endothermic reaction.

Since the force of attraction between adsorbate and adsorbent releases heat energy when ΔG is negative, it follows that adsorption is a spontaneous process. The interaction of MB and metal ions and, thus, adsorption, occurs in the liquid phase due to lower porosity, as confirmed by nitrogen adsorption. The challenge is to re-structure metal compounds themselves to encourage stronger interaction with MB. The quantity of desorbed water molecules is greater than the quantity of adsorbed MB molecules (dyes are bulky compared with water, which shows that water molecules may be desorbed via the adsorption of the dye molecules). Moreover, the driving force of dye adsorption ($-\Delta G$) on metal is by means of entropy (max. $+\Delta S$) instead of enthalpy change (positive ΔH). The adsorption of MB at various temperatures is a spontaneous and endothermic process where randomness increases during the interaction of metal and MB, i.e., adsorption. On the other hand, entropy increases with increasing temperature.

7. Temperature Analysis

The behavior of adsorption can be significantly influenced by temperature, which is a significant parameter. The analysis of the exothermic and endothermic behaviors of adsorption requires knowledge of both temperature and adsorption data. The outcomes can be categorized as exothermic and endothermic processes, respectively.

When wheat husk was applied for the removal of MB dye, the percentage of MB removed decreased from 93.4 to 59.8% (from 303 K to 323 K), which signified exothermic behavior. At high temperatures, the escape properties of the dye molecule were high, as described in Figure 8 [13]. When the study was carried out at temperatures of 30, 40, 50, and 60 °C, similar exothermic behavior was observed, indicating that the increment in adsorption capacity corresponded directly to a decrease in temperature; lower temperatures were favorable for biosorption when cone powder was used, as shown in Figure 9 [43]. The increment in temperature was inversely proportional to the decrement in the adsorption of MB dye molecules. The decreased surface area reflected the exothermic nature of the adsorption of MB on pinecones. As the surface area decreased, the heat was released.

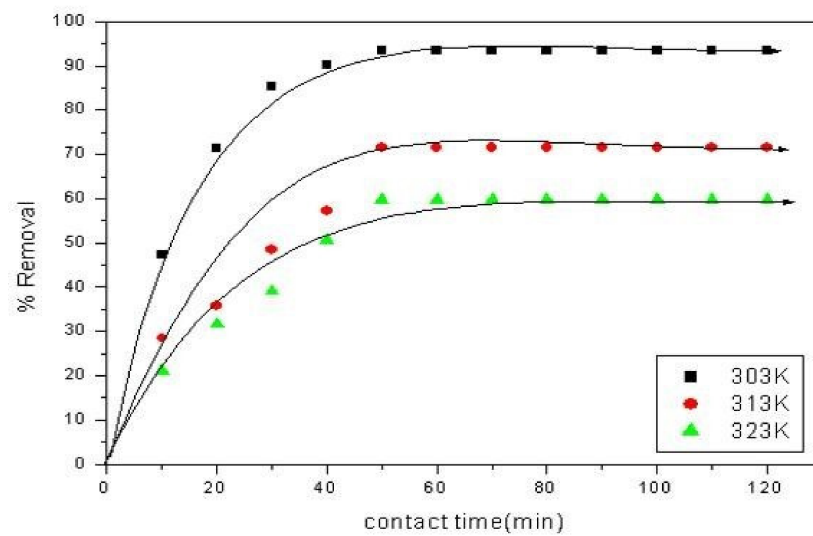


Figure 8. Modified wheat husk [13].

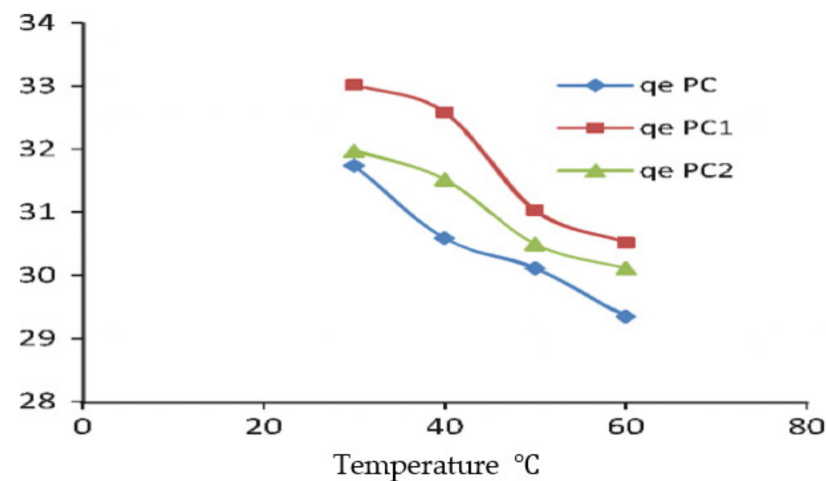


Figure 9. Biosorption when cone powder was used. PC: pinecone, PC1: modified pinecone with 0.1 M, PC2: modified pinecone with 0.05 M NaOH [43].

As the temperature increased, the attractive forces between the pinecone biomass surface and the dye weakened. Such behavior reflects the escape capacity of the dye from the solid phase of biomass toward the liquid phase while using *Pinus radiata*, as analyzed by the graph in Figure 10 [30]. The percentage of MB removed as the temperature decreased from 30 to 50 °C ranged from 93.2 to 99.16%, which signifies endothermic behavior during the application of carbon prepared from rice [12]. Table 3 also shows that the increment in the removal of MB was directly proportional to the increment in temperature, which indicates an endothermic process. The rate of diffusion of the dye molecule within the external boundaries of the layer or internal pores of the adsorbent particle decreased with changes in the viscosity rate while using *Ephedra strobilaceous* sawdust, as represented in Figure 11 [39]. A similar behavior of decreasing viscosity and density while the rate of diffusion increased was observed when modified sawdust was applied for the removal of MB [32]. Endothermic behavior has been defined as a valuable concept, whereas adsorption behavior is defined as being due to magnifying pores as the temperature increases in order to capture cationic dye and decrease the swelling effect [29].

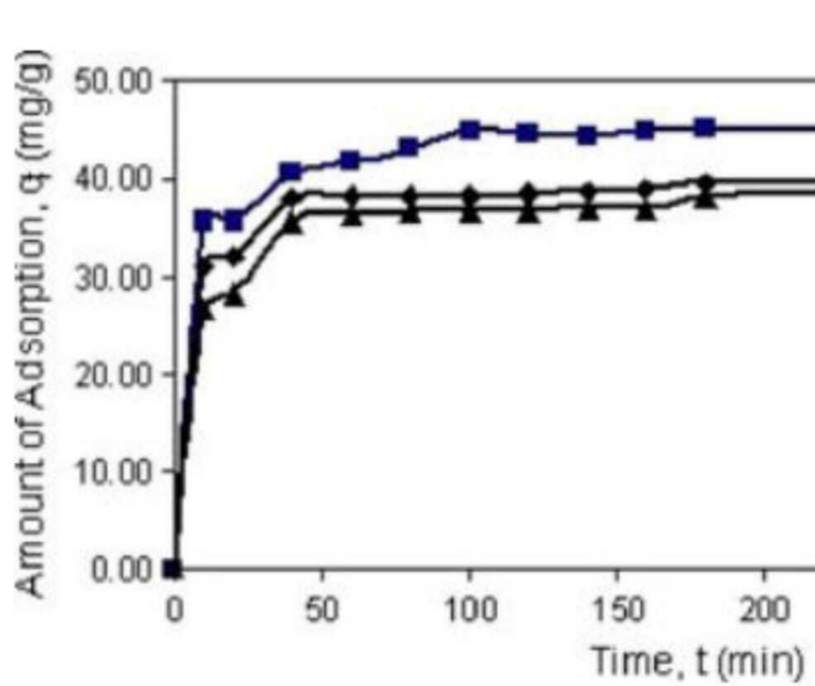


Figure 10. Effect of temperature on the adsorption of MB onto pinecone powder [30].

Table 3. Thermodynamic properties studied during MB removal.

Adsorbent	Temperature (K)	ΔG (kJ mol ⁻¹)	ΔH (kJ mol ⁻¹)	ΔS (kJ mol ⁻¹ K ⁻¹)	Reference
Raw pinecone	303	-13.64	-14.61	-0.017	[43]
	313	-13.12	-14.16	-0.017	
	323	-0.017	-0.017	-0.017	
Pine sawdust (<i>Pinus tabulaeformis</i>)	293	-12.68	1.899	0.495	[32]
	303	-12.95			
	313	-13.67			
<i>Pinus radiata</i>	303	-7.56	-26.50	-0.062	[30]
	318	-6.63	-26.50	-0.062	
	333	-5.69	-26.50	-0.062	
Sugar extracted from spent rice biomass (<i>Ficus carica</i> bast) FCBAC	298	-1314	1568	9.67	[34]
	323	-1508			
NaOH-modified rejected tea	303	-9.823	7.169	56.082	[41]
	313	-11.049			
	323	-11.941			
Carbonized plant leaf powder from teak (<i>Tectona grandis</i>) and guava (<i>Psidium guajava</i>) trees	293	-21,650.	23,146.4	153.1	[20]
	303	-23,323.6			
	313	-24,748.1			
	323	-26,270.6			
Raw <i>Spirogyra</i> sp. (green alga)		-20.89	-15.03	0.02	[36]
Pretreated <i>Spirogyra</i> sp. (green alga)		-19.24	-13.38	0.02	

Table 3. Cont.

Adsorbent	Temperature (K)	ΔG (kJ mol ⁻¹)	ΔH (kJ mol ⁻¹)	ΔS (kJ mol ⁻¹ K ⁻¹)	Reference
OTPW	298	-26.97	-11.85	+0.051	[28]
	333	-28.75		+0.051	
COTPW	298	-28.07	-30.93	-0.010	
	333	-27.73		-0.010	
ESC	298	-20.79	17.44	0.128	
	308	-22.29			
	318	-23.58			
	328	-24.97			
ESP	298	-19.43	12.04	0.105	[39]
	308	-20.39			
	318	-21.60			
	328	-22.78			
ESZ	298	-18.76	17.39	0.121	
	308	-19.87			
	318	-21.90			
	328	-22.71			

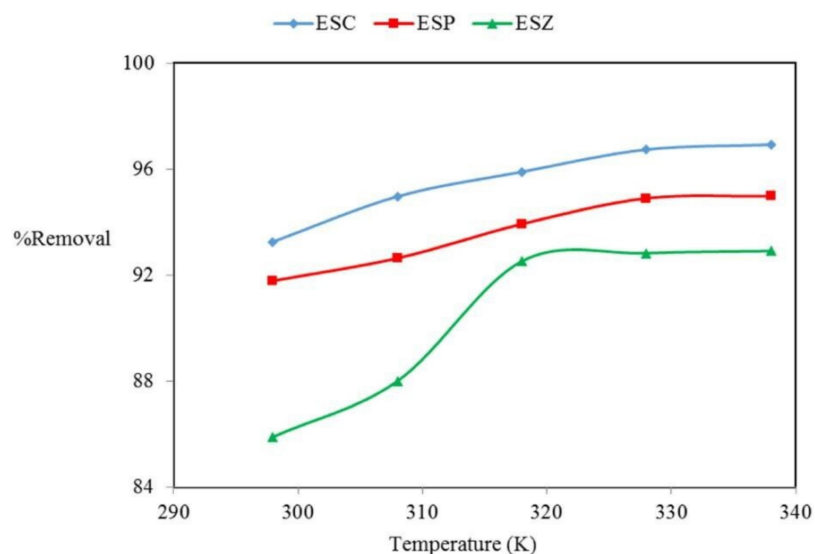


Figure 11. ESC: Ephedra strobilacea char. ESP: *E. strobilacea* char modified using phosphoric acid. ESZ: *E. strobilacea* char zinc chloride. *Ephedra strobilacea* sawdust modified using phosphoric acid and zinc chloride [3].

8. pH

The adsorption process is critically dependent on pH. Adsorption increased within a pH range of 3–6 when the experiment was run using the m-ALG/RH bio-composite as an adsorbent. However, no significant changes were observed within the range of 6–10 [11]. Similar behavior was observed when wheat husk was used as an adsorbent; the rate of adsorption was directly proportional to pH ranges at 13.37×10^{-2} mol/L [13]. As such, the removal rate for MB changed from 40.7 to 96.2% by increasing pH from 4.5 to 9.5. Elmorsi described an interesting phenomenon whereby the adsorption rate was at its maximum in a basic medium. This is because the degree of ionization of the dye molecules affects interaction with the surface properties of the adsorbent. Observations on miswak leaves

revealed 60.9 mg/g of adsorption at a pH of 10.6 versus 13.54 mg/g at a pH of 2.8, which proves that a pH of 10.6 is a favorable condition for adsorption [67]. As per an experiment with pine (*Pinus Durangensis*) (NS) sawdust, the adsorption of MB onto NS increased by 1.7, 2.0, and 4.6 times when the pH was raised from 3 to 4.25, from 3 to 7, and from 3 to 10, respectively; these results show that adsorption increases at higher pH ranges [14].

Adsorption experiments with different adsorbents have shown that a basic medium or higher pH provides a favorable environment for adsorption. This is due to a higher concentration of H^+ at lower pH levels, which interferes with the adsorption process. Generally, an ion exchange of H^+ ions signifies the adsorption of MB via electrostatic attraction, where the basic medium conveys a significant negative charge to adsorbent surfaces interfacing with cationic dye (MB), i.e., increases in adsorption rate.

9. Adsorbent Dosage

When m-ALG/RH bio-composite was utilized as an adsorbent, the adsorption of MB rose from 15 to 89% with an increase in the amount of adsorbent from 145 to 338 mg/g, and thus an increase in the level of interaction between MB and the adsorbent [11]. Similarly, the study was carried out using wheat husk with 10, 20, and 25 g/L of the adsorbent and an initial MB concentration of 13.37×10^{-2} mol/L at 303 K. The adsorption of MB increased from 79.80 to 93.4% with the increase from 10 to 25 g/L. The study was also conducted using miswak leaves, with adsorbent quantities ranging from 0.5 to 3.0 g/L for MB dye adsorption [13]. Initially, adsorption capacity increased slowly with the adsorbent dose. It was observed that 1.0 g/L of adsorbent was the point at which the maximum capacity of 60.90 mg/g was reached. Hence, increasing the amount of miswak leaves up to 1.0 g can be credited with the increase in both surface area and the number of adsorption sites for MB dye molecules [67]. This experiment yielded the same result when RHAC was used; an increment in the adsorption rate from 86.75 to 99.83% was observed with an increase in the amount of adsorbent from 0.40 to 0.60 g when 50 mL of dye solution was used. As expected, a higher rate of dye removal was obtained at increased adsorbent doses [12].

Therefore, an increment in the adsorption of MB is achieved with a higher dose of adsorbent; this is because higher adsorbent dosages are directly proportional to an increase in surface sites for MB, which leads to excellent adsorption.

10. Initial Dye Concentration and Contact Time

In one experiment, the starting MB concentration was raised from 25 to 500 mg/L, which is comparable to an increase of 465.6%, using m-ALG/RH bio-composite beads as the adsorbent. The experiment revealed that the maximal adsorption capacity was 274.9 mg/g, which is an important piece of information. Temperatures from 293 to 333K were used for the contact period, and the amounts of MB that were adsorbable were 53.4 and 36.9 mg/g, respectively [11]. When miswak leaves were used, variation was observed. Initially, at 10 min, adsorption had incremented 9.4 times (from 16 to 150 mg/L). As contact time increased to 30min, adsorption increased sevenfold (from 9.01 to 62.13 mg/g) [67]. While RHAC was used as an adsorbent to measure the percentage of dye removal in relation to contact time, initial concentrations ranged from 60 to 100 mg/L; the removal of MB needed 100 min for equilibrium and became increasingly steady for maximum efficiency. The adsorption was fast at first and achieved a certain equilibrium; then, no more adsorption occurred. For the initial concentration of 60 mg/L, adsorption increased from 82.75 to 93.2%, with a decrement in the initial concentration of MB from 100 to 60 mg/L [12]. The maximum adsorption was achieved at an initial concentration of 60 mg/L and at 303 K. The initial concentrations of MB tested were 13.37×10^{-2} , 20.06×10^{-2} , 26.74×10^{-2} , and 33.43×10^{-2} mol/L [13].

Adsorption occurred over different durations of time for different initial concentrations because the dye took a different amount of time to attain equilibrium, which happened after encountering the boundary layer effect. Once the dye reached the surface of the adsorbent,

it diffused into the pores of the adsorbent. With the number of sites being saturated by higher initial levels of MB, the dye removal percentage decreased.

11. BET Surface Area

BET analysis is known as the best method for determining surface area; it uses the N₂ adsorption isotherm, which was derived via multi-layer gas adsorption on flat surfaces (Table 4).

Table 4. BET Surface Area of various adsorbent.

Adsorbent	BET Surface Area (m ² /g)	Reference
RHAC	180.50	[12]
Wheat husk	81.75	[13]
MPAC-5	1832	[66]

12. Adsorption Isotherm

For the purpose of simulating adsorption behavior, specific types of equations have been developed. Adsorption equilibrium is examined using the Langmuir, Freundlich, Redlich-Peterson, and Dubinin-Radushkevich models. In investigations where CAMS was utilized as an adsorption agent, equilibrium data and fitted equilibrium curves are shown in Figure 12. Multiple isotherm models were used for this at various temperatures [32].

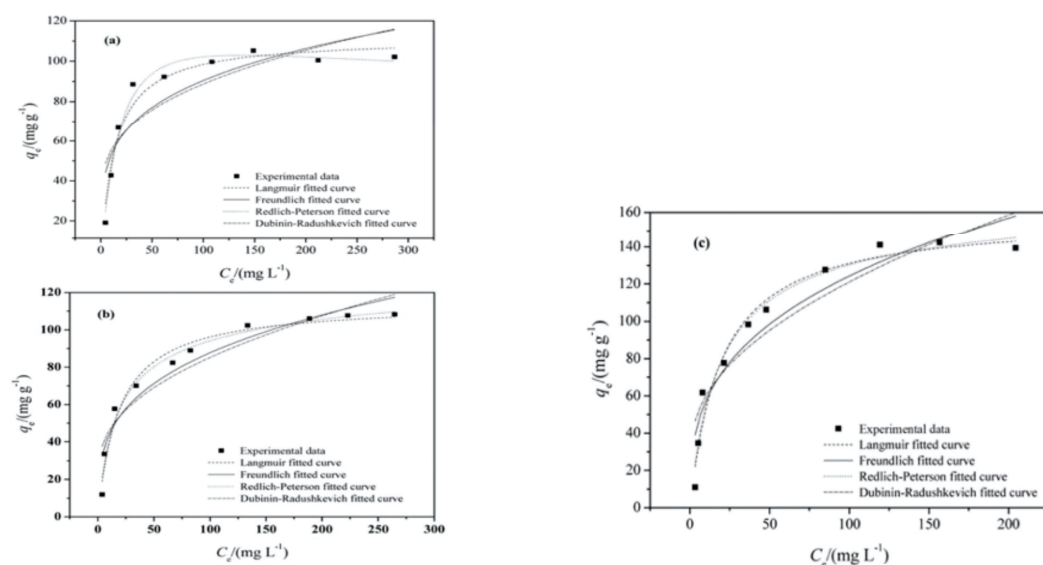


Figure 12. Langmuir and Freundlich model of MB adsorption on sawdust [32]. (a) monolayer MB (b) HA/Au nanocomposite adsorbent agent (c) miswak leaves.

Here, the Freundlich constant (K_F) decreased the value of $1/n$ with an increment in temperature. On the other hand, the Redlich–Peterson parameters (g) were nearer to 1, which indicated that the Langmuir model was better than the Freundlich model. As analyzed by the Dubinin–Radushkevich model, the magnitude of the adsorption energy (E) was more than 8 kJ mol⁻¹ for all temperatures, which reflected chemical adsorption characterized by monolayer MB covering the surface of the adsorbent [32]. A similar study was carried out using an HA/Au nanocomposite adsorbent agent, where the correlation coefficient of the Freundlich isotherm ($R^2 = 0.873$) was lower than that of the Langmuir isotherm, which would indicate that the adsorption of dye on the surface was homogenous shown in Figure 13 [68]. It showed a smooth and linear path that was in accord with the equilibrium data for Langmuir’s model. The Freundlich isotherm’s correlation coefficient exceeded 0.99, in contrast to Langmuir’s correlation coefficient ($R^2 < 0.98$). So, monolayer

adsorption pointed toward the Freundlich model, i.e., 9.83 mg/g at 30 °C [12]. When a study of MB adsorption was carried out using miswak leaves at 30 °C, the linear form of the Langmuir model showed the least deviation from the fitted equation, as reflected by the high R^2 value of 0.999, which indicated a monolayer. The value of $1/n$ (indicative of favorability) was 0.85, which was appropriate for unity, i.e., favorable for the adsorption process. Thus, the Freundlich model is a good tool for describing adsorption [67].

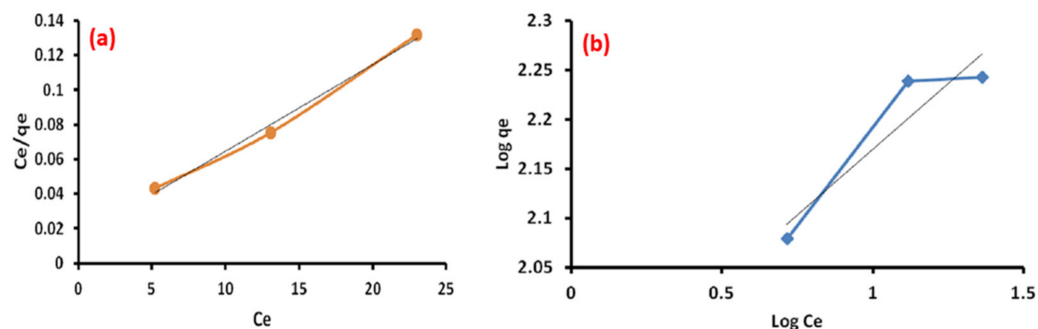


Figure 13. Hydroxyapatite/gold nanocomposite to adsorb MB: (a) Langmuir isotherm model; (b) Freundlich isotherm model [68].

The equilibrium adsorption isotherm was examined by plotting the solid-phase concentration against the liquid-phase concentration. In this review, Langmuir's and Freundlich's adsorption isotherm models were used to examine equilibrium data with respect to the removal of dye. In Langmuir's adsorption isotherm model, a number of molecules are evenly adsorbed by an equal number of surface sites. There is no interaction between adsorbate molecules once all sites are occupied. Because there is no interaction, the adsorption energy of the respective molecules is constant.

The Freundlich model concerns non-ideal multi-layer sorption onto heterogeneous surfaces via uniform energy distribution, i.e., it includes a reversible adsorption property. It is known that the values of K_F and n increase with increases in temperature for the adsorption of MB, which resembles a favorable environment for adsorption at high temperatures. When the value of $n = 1$, the result is a linear isotherm. If the value of $n < 1$ or $n > 1$, then it is chemical or physical adsorption, respectively.

13. Kinetic Study

Three methods—the pseudo-first-order, the pseudo-second-order, and the Elovich equation—can be used to estimate a kinetic model. Many writers conduct analysis using pseudo-first-order and pseudo-second-order kinetic models. HA/Au nanocomposite is applied as adsorbent of MB then pseudo-first-order and pseudo-second-order kinetic models are employed for evaluating kinetic where the theoretical value of pseudo-first-order matches with experimental value but the theoretical value of pseudo-second-order kinetic model has a high variation with the experimental value. On the other hand, the correlation coefficient (R^2) of pseudo-first-order is higher than that of pseudo-second-order. Hence, the pseudo-first-order model fitted with experimental data which resembles the process involved in physisorption where dye molecule interacted with adsorbent via electrostatic attraction of functional group of adsorbent shown in Figure 14 [68]. When CAMS is applied as an adsorbent then the Elovich equation shows a high degree of fitting which resembles that CAMS means of adsorption is chemical adsorption which takes part in the ion exchange process. Hereby, ion exchange reflects that MB exit as a positive charge whereas the carboxyl group (-COO-) exists as a negative charge shown in Figure 15 [32]. A similar observation is observed in miswak leaves, where the theoretical value of pseudo-first-order doesn't fit with the experimental value which resembles the similar kinetic behavior as HA/Au nanocomposite [67]. Even, a pseudo-second-order kinetic model is also respected via wheat husk [13].

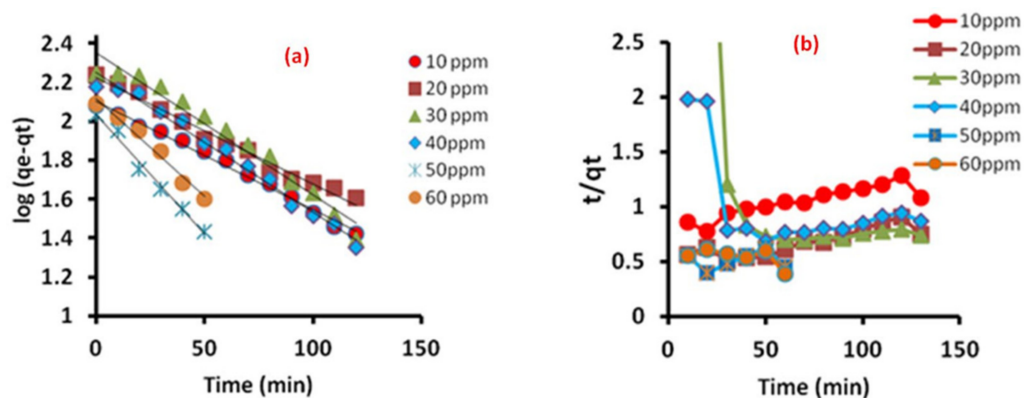


Figure 14. Kinetic study on dye adsorption of MB on HA/ Au. (a) Pseudo- first order and (b) pseudo-second-order kinetic model for dye adsorption of MB on HA/ Au [68].

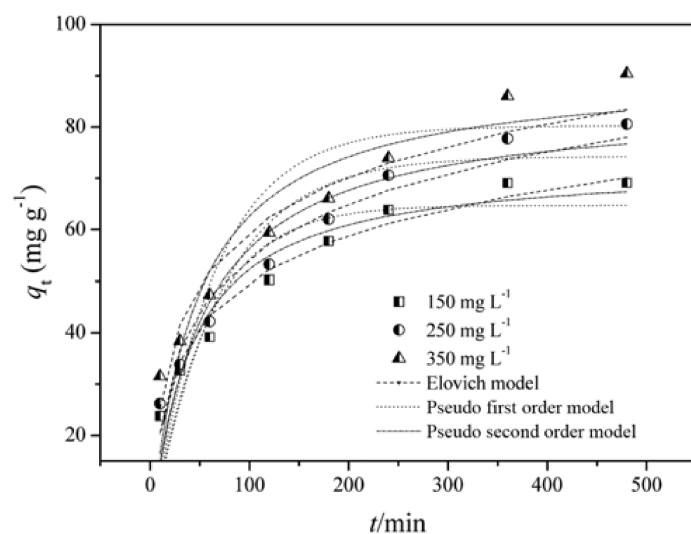


Figure 15. Kinetic study of adsorption of MB onto CAMS at 293 K [32].

Indeed, the pseudo-second-order kinetic model is useful for many agricultural products for which its correlation values are higher than those of the pseudo-first-order model. For the values to be acceptable, the theoretical data must match the experimental data.

14. EDX

For elemental analysis, the EDX method is used. For instance, EDX demonstrates the existence of Ca and P according to their maximum concentration. The presence of AuNPs on the surface of HA demonstrates proper AuNP collaboration inside the HA matrix. When biologically activated banana peel waste was applied as an adsorbent, EDS was used to analyze the elemental composition before and after the adsorption of MB. After the adsorption, increases in nitrogen and sulfur peaks confirmed MB adsorption; such peaks were absent before MB adsorption [69]. When rice (*Oryza sativa* L.) straw biosorbent (RSB) was used as an adsorbent, differences were observed before and after MB adsorption. C, O, and some amounts of Si and Ni were initially detected, whereas after the adsorption of MB by the RSB, the surface was smooth and compact, and the amounts of C, O, and N had increased [70].

When alginate-based beads were used as the adsorbent, EDX was only applied to analyze the relevant elements, i.e., C, O, Fe, Cu, and Ca. EDX is typically employed for confirmation of elemental analyses. For adsorption, however, it must be used both before and after adsorption studies in order to confirm the presence of relevant elements and encourage the authors to pursue a detailed study.

15. XRD

Figure 16 shows the XRD analyses of apricot stones (AS) and citric-acid-treated apricot stones (CA-AS). There were no differences observed before or after citric acid treatment. Two peaks, one at 21.94 and one at 34.9, reflect the cellulosic structure. The interesting factor that needs to be noted from the peaks is that even after esterification, citric acid was unable to damage the crystal structure of the cellulose [71].

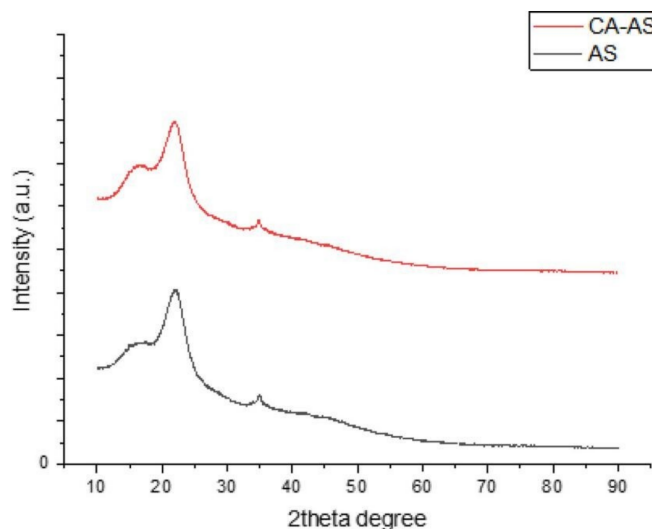


Figure 16. XRD pattern of AS and CA-AS [71].

16. Mechanisms of Using Agriculture Products as Adsorbents of MB

Complexation, ion exchange due to surface ionization, and hydrogen bonding are only a few examples of the various interactions that are involved in chemical bonding and the ion exchange method. The ability of MB to create a covalent link with the cellulose of agricultural products is an intriguing characteristic.

An interesting property of MB is that it forms a covalent bond with the cellulose of agricultural products. Table 2 confirms, for various products, the functional groups of cellulose. Generally, pH, adsorbent dose, dye concentration, and contact time are known as functions of the equilibrium adsorption level. The Freundlich and Langmuir isotherms can be employed to determine the equilibrium adsorption level. Finally, many varieties of agricultural waste have been tested for suitability for dye removal. The findings regarding adsorption capacity vary according to the experiment. Nevertheless, this review clarifies that agricultural waste and nanoparticles formed from agricultural waste are inexpensive, readily available, and effective reagents. In addition, this review focuses on eco-friendly materials with high adsorption capacities that have been selected for suitability for different concentrations and the best kinetics [72].

17. Nanoparticles Formed Using Agricultural Products

Agricultural products can be used to produce nanoparticles and act as adsorbents for MB, making their production sustainable, affordable, and friendly to the environment. The biosynthesis of Au via the *Acrocarpus fraxinifolius* HA/Au nanocomposite can be applied for the removal of dyes; this reflects the thermodynamic modeling that showed that the adsorption process was spontaneous and endothermic. A value of $+\Delta S^\circ$ shows the activity of the surface of the HA/Au nanocomposite surface toward dye [68].

The production of zirconium oxide nanoparticles was carried out using a pericarp extract of *S. mukorossi*, having a size of 10 nm. It can adsorb 0.3 g with an initial MB concentration of 20 mg/L and an average time duration of 300 min. The thermodynamic study conducted herein reflected the endothermic and spontaneous nature of the process,

representing a form of activation energy. On the other hand, nano zirconia exhibited a regenerative capacity for adsorbing MB [61].

Nickel oxide nanoparticles were prepared via an extract of *Zizyphus jujuba* fruit having a size range of 5–30 nm; they were able to degrade MB dye by 65.5%, which reflects the application of these nanoparticles in industrial wastewater purification [73].

Magnetic nanoparticles (Fe_3O_4) were formed via the chemical precipitation of a mixture of Fe^{2+} and Fe^{3+} salts. XRD confirmed the inverse cubic spinel structure of the nanoparticle form of Fe_3O_4 using wheat straw in crystal form. As per the SEM report for nano- Fe_3O_4 , the particles showed spherical and cage-like structures and paramagnetic properties, indicating a favorable pathway for adsorption. FT-IR showed the presence of cellulose having -OH that binds, via electrostatic attraction, with MB dye [62].

In addition, α -chitin nanoparticles were formed via shells of *P. monodon*. As per temperature analysis, the adsorption of dye increased slightly with increases in temperature, which indicated an endothermic process. Hence, dye adsorption was high at higher temperatures. FT-IR showed a band at -OH ranges due to the presence of fiber, i.e., the physical adsorption of MB [74].

In the field of clean water science, adsorption is a promising technology. Numerous studies have been conducted on nanoparticles such as TiO_2 , ZnO , and Fe_3O_4 that can be used for MB degradation [75]. Silica nanoparticles were prepared from rice husk using microwave technology to update the nature of the material's behavior to remove MB from aqueous solutions. FT-IR spectra showed 3430, 1635, 1080, 800, and 460 cm^{-1} , where 3430 cm^{-1} is known to reflect vibrations of O-H or SiO-H groups; this result supported the confirmation of MB adsorption. As per thermodynamic analysis, van der Waals interactions were less than 20 kJ mol^{-1} , whereas electrostatic interactions ranged from 20 to 80 kJ mol^{-1} , reflecting bond strengths of 80-450 kJ mol^{-1} . These results favored the formation of chemical bonds between MW-nSiO₂ and MB [76].

These nanoparticles can be prepared either industrially or in a laboratory and can be used for further studies on MB adsorption due to their simplicity, flexibility, and versatility.

Compared to other tested adsorbents, nanomaterials are noteworthy and attractive adsorbents due to their higher specific area and, in most cases, higher adsorption capacity for target pollutants. Parameters such as initial concentration, thermodynamics, functional properties, and temperature were found to control the adsorption process. In terms of thermodynamics, the entropy- and enthalpy-based phenomena varied as the material varied. A number of articles about nanomaterials discuss issues relevant to nano-adsorbents in terms of multi-metal composition and their application in the treatment of wastewater. Although adsorption is difficult to analyze, a multi-factor analysis is important. For most nanoparticles, there exists either a chemical treatment or an indigenous method of preparation that must be the focus of a pilot project or an entrepreneurial approach in order to make progress toward a real adsorption pathway.

18. Future Prospects Wait

This review focused on domestic resources that are readily available and inexpensive and, consequently, could easily be used by developing and under-developed countries to mitigate the MB problem. Promoting this approach at the industrial level will require further research. Future studies should include costing evaluations, technical feasibility assessments, and engineering evaluations to not only reduce costs but also increase output. To connect the experimental data with real-world applications, a pilot project is required. In the process, such an endeavor would encourage local researchers to explore locally available resources and to “think globally, act locally” in an eco-friendly manner.

Additionally, zeolitic imidazolate frameworks are used to adsorb pollutant metals [76]. Phenyl diazene-based metal complexes should be preferred because they have antibacterial and antifungal properties [77]. The phenyl diazene azo compound has led to many innovations in the 21st century [78]. Indigenous sources, such as biochar made from bamboo or aquatic plants such as *Azolla pinnata* (AP), must be targeted for use in the adsorption of MB [79,80].

19. Conclusions

Water and wastewater colouring caused by the dyeing industry is a serious issue on a global scale. Agricultural products and the nanoparticles they are associated with play a promising role among the simple, affordable, and effective adsorption strategies that could be used to address this issue. It has been shown throughout this review work that there are readily available agricultural products that can remove MB.

Functional group determinations by FT-IR and surface examinations via SEM confirmed the role of -C=O and -OH for the binding of positive cationic dye, i.e., MB, usable either in normal or nanoparticle forms. The rate of adsorption increased with an increase in initial concentration and reached equilibrium before decreasing. A basic medium was favorable for high adsorption. Based on a high correlation factor, the pseudo-second-order model fit well within the context of the examined agricultural products. The results also respected the Langmuir adsorption isotherm. It was interesting to find that temperature showed either endothermic behavior or exothermic behavior, depending on the material. The thermodynamic parameters (enthalpy, entropy, and Gibbs free energy) also showed major activity; these results support the future promise of fruitful action and visionary applications.

Author Contributions: Conceptualization, M.K.S. and A.B.; writing—original draft preparation, K.E., A.E.-H., S.A., L.M.; writing—review and editing, M.K.S., T.S.A., N.A. and A.B.; funding acquisition, K.E., T.S.A.; supervision, T.S.A., N.A. and A.B. All authors have read and agreed to the published version of the manuscript.

Funding: This research received no external funding.

Conflicts of Interest: The authors declare no conflict of interest.

Abbreviations

MB	Methylene blue
FT-IR	Fourier transform infrared
SEM	Scanning electron microscope
EDX	Energy dispersive X-ray spectroscopy
BET	Brunauer–Emmette–Teller
OL	Organosolv lignin
OTPW	Olive tree pruning wastes
FCBAC	Ficus carica activated carbon
TSA	Tobacco stem ash
EDTA	Ethylenediaminetetraacetic acid
EDTAD	EDTA dianhydride (EDTAD)
Q_m	Langmuir sorption ability
NRH	Natural rice husk
MRH	Modified rice husk
MPAC	Mangosteen peel activated carbon
NS	Natural white pine sawdust
GNSP	Groundnut shell powder
CAMS	Citric-acid-modified sawdust
SRB	Spent rice biomass
-NH	Amido groups
R-RT	Raw rejected tea
N-RT	NaOH-modified rejected tea
m-ALG/RH	Magnetic alginate/rice husk
MWH	Modified wheat husk
OTPW	Olive tree pruning waste
COTPW	Composted olive tree pruning waste
K_F	Freundlich constant
E	Adsorption energy
RHAC	Rice husk activated carbon

References

1. Chowdhury, S.; Das, P. Biosorption of methylene blue from aqueous solutions by a waste biomaterial: Hen feathers. *Appl. Water Sci.* **2012**, *2*, 209–219. [[CrossRef](#)]
2. Shih, M.-C. Kinetics of the batch adsorption of methylene blue from aqueous solutions onto rice husk: Effect of acid-modified process and dye concentration. *Desalin. Water Treat.* **2012**, *37*, 200–214. [[CrossRef](#)]
3. Al-Tohamy, R.; Ali, S.S.; Li, F.; Okasha, K.M.; Mahmoud, Y.A.-G.; Elsamahy, T.; Jiao, H.; Fu, Y.; Sun, J. A critical review on the treatment of dye-containing wastewater: Ecotoxicological and health concerns of textile dyes and possible remediation approaches for environmental safety. *Ecotoxicol. Environ. Saf.* **2022**, *231*, 113160. [[CrossRef](#)]
4. Golka, K.; Kopps, S.; Myslak, Z.W. Carcinogenicity of azo colorants: Influence of solubility and bioavailability. *Toxicol. Lett.* **2004**, *151*, 203–210. [[CrossRef](#)]
5. Lee, S.-K.; Mills, A. Novel photochemistry of leuco-Methylene Blue. *Chem. Commun.* **2003**, 2366–2367. [[CrossRef](#)]
6. Crettaz, S.; Kämpfer, P.; Brüscheiler, B.J.; Nussbaumer, S.; Deflorin, O. Survey on hazardous non-regulated aromatic amines as cleavage products of azo dyes found in clothing textiles on the Swiss market. *J. Consum. Prot. Food Saf.* **2019**, *15*, 49–61. [[CrossRef](#)]
7. Rafatullah, M.; Sulaiman, O.; Hashim, R.; Ahmad, A. Adsorption of methylene blue on low-cost adsorbents: A review. *J. Hazard. Mater.* **2010**, *177*, 70–80. [[CrossRef](#)]
8. Ahmad, A.; Mohd-Setapar, S.H.; Chuong, C.S.; Khatoun, A.; Wani, W.A.; Kumar, R.; Rafatullah, M. Recent advances in new generation dye removal technologies: Novel search for approaches to reprocess wastewater. *RSC Adv.* **2015**, *5*, 30801–30818. [[CrossRef](#)]
9. Kini, M.S.; Saidutta, M.B.; Murty, V.R. Studies on Biosorption of Methylene Blue from Aqueous Solutions by Powdered Palm Tree Flower (*Borassus flabellifer*). *Int. J. Chem. Eng.* **2014**, *2014*, 306519. [[CrossRef](#)]
10. Adelodun, B.; Ajibade, F.; Abdulkadir, T.; Bakare, H.; Choi, K. SWOT analysis of agro-waste based adsorbents for persistent dye pollutants removal from wastewaters. *Environ. Degrad. Causes Remediat. Strateg.* **2020**, 88–103. [[CrossRef](#)]
11. Alver, E.; Metin, A.; Brouers, F. Methylene blue adsorption on magnetic alginate/rice husk bio-composite. *Int. J. Biol. Macromol.* **2020**, *154*, 104–113. [[CrossRef](#)] [[PubMed](#)]
12. Sharma, Y.C.; Uma; Upadhyay, S.N. An economically viable removal of methylene blue by adsorption on activated carbon prepared from rice husk. *Can. J. Chem. Eng.* **2011**, *89*, 377–383. [[CrossRef](#)]
13. Banerjee, S.; Chattopadhyaya, M.C.; Uma; Sharma, Y.C. Adsorption Characteristics of Modified Wheat Husk for the Removal of a Toxic Dye, Methylene Blue, from Aqueous Solutions. *J. Hazard. Toxic Radioact. Waste* **2014**, *18*, 56–63. [[CrossRef](#)]
14. Salazar-Rábago, J.J.; Leyva-Ramos, R.; Rivera-Utrilla, J.; Ocampo-Perez, R.; Cerino-Cordova, F. Biosorption mechanism of Methylene Blue from aqueous solution onto White Pine (*Pinus durangensis*) sawdust: Effect of operating conditions. *Sustain. Environ. Res.* **2017**, *27*, 32–40. [[CrossRef](#)]
15. Ahmad, H.B.; Anwar, T.; Ashiq, M.N.; Yousaf, M.; Aleem, M. Comparative studies for the adsorption of remazol blue on rice husk, saw dust and charcoal. *J. Chem. Soc. Pak.* **2011**, *33*, 449–453.
16. Patil, S.; Renukdas, S.; Patel, N. Removal of methylene blue, a basic dye from aqueous solutions by adsorption using teak tree (*Tectona grandis*) bark powder. *Int. J. Environ. Sci.* **2011**, *1*, 711–726.
17. Ong, S.; Keng, P.; Voon, M.; Lee, S. Application of durian peel (*Durio zibethinus* Murray) for removal of methylene blue from aqueous solution. *Asian J. Chem.* **2011**, *23*, 2898–2902.
18. Dharmalingam, V.; Ramasamy, A.K.; Balasuramanian, V. Chemical Modification on Reactive Dye Adsorption Capacity of Castor Seeds. *E-J. Chem.* **2011**, *8*, S335–S343. [[CrossRef](#)]
19. Vargas, A.M.M.; Cazetta, A.L.; Kunita, M.H.; Silva, T.L.; Almeida, V.C. Adsorption of methylene blue on activated carbon produced from flamboyant pods (*Delonix regia*): Study of adsorption isotherms and kinetic models. *Chem. Eng. J.* **2011**, *168*, 722–730. [[CrossRef](#)]
20. Gunasekar, V.; Ponnusami, V. Kinetics, Equilibrium, and Thermodynamic Studies on Adsorption of Methylene Blue by Carbonized Plant Leaf Powder. *J. Chem.* **2013**, *2013*, 415280. [[CrossRef](#)]
21. Gunasekar, V.; Kumar, S.; Ponnusami, V. Prediction of Adsorption Kinetic Rate Constant for Removal of Methylene Blue Using Teak Leaf Powder. *Asian J. Sci. Res.* **2014**, *7*, 284–293. [[CrossRef](#)]
22. Fiaz, R.; Hafeez, M.; Mahmood, R. *Ficus palmata* leaves as a low-cost biosorbent for methylene blue: Thermodynamic and kinetic studies. *Water Environ. Res.* **2019**, *91*, 689–699. [[CrossRef](#)]
23. Dural, M.U.; Cavas, L.; Papageorgiou, S.K.; Katsaros, F.K. Methylene blue adsorption on activated carbon prepared from *Posidonia oceanica* (L.) dead leaves: Kinetics and equilibrium studies. *Chem. Eng. J.* **2011**, *168*, 77–85. [[CrossRef](#)]
24. Mathivanan, M.; Saranathan, E.S. Sugarcane bagasse-a low cost adsorbent for removal of methylene blue dye from aqueous Solution. *J. Chem. Pharm. Res.* **2015**, *7*, 817–822.
25. Nharingo, T.; Shoniwa, V.; Hunga, O.; Shumba, M. Exploring the biosorption of methylene blue dye onto acid treated sugar-cane bagasse. *Int. J. Curr. Res.* **2013**, *5*, 2169–2175.
26. Kumar, S.; Gunasekar, V.; Ponnusami, V. Removal of Methylene Blue from Aqueous Effluent Using Fixed Bed of Groundnut Shell Powder. *J. Chem.* **2013**, *2013*, 259819. [[CrossRef](#)]
27. Zhang, S.; Wang, Z.; Zhang, Y.; Pan, H.; Tao, L. Adsorption of Methylene Blue on Organosolv Lignin from Rice Straw. *Procedia Environ. Sci.* **2016**, *31*, 3–11. [[CrossRef](#)]

28. Anastopoulos, I.; Margiotoudis, I.; Massas, I. The use of olive tree pruning waste compost to sequester methylene blue dye from aqueous solution. *Int. J. Phytoremediation* **2018**, *20*, 831–838. [[CrossRef](#)]
29. Pathania, D.; Sharma, S.; Singh, P. Removal of methylene blue by adsorption onto activated carbon developed from *Ficus carica* bast. *Arab. J. Chem.* **2017**, *10*, S1445–S1451. [[CrossRef](#)]
30. Sen, T.K.; Afroze, S.; Ang, H.M. Equilibrium, Kinetics and Mechanism of Removal of Methylene Blue from Aqueous Solution by Adsorption onto Pine Cone Biomass of *Pinus radiata*. *Water Air Soil Pollut.* **2010**, *218*, 499–515. [[CrossRef](#)]
31. Ghosh, R.K.; Reddy, D.D. Tobacco Stem Ash as an Adsorbent for Removal of Methylene Blue from Aqueous Solution: Equilibrium, Kinetics, and Mechanism of Adsorption. *Water Air Soil Pollut.* **2013**, *224*, 1582. [[CrossRef](#)]
32. Zou, W.; Bai, H.; Gao, S.; Li, K. Characterization of modified sawdust, kinetic and equilibrium study about methylene blue adsorption in batch mode. *Korean J. Chem. Eng.* **2013**, *30*, 111–122. [[CrossRef](#)]
33. Zhang, R.; Zhou, Y.; Gu, X.; Lu, J. Competitive Adsorption of Methylene Blue and Cu^{2+} onto Citric Acid Modified Pine Sawdust. *CLEAN Soil Air Water* **2014**, *43*, 96–103. [[CrossRef](#)]
34. Rehman, M.S.U.; Kim, I.; Han, J.-I. Adsorption of methylene blue dye from aqueous solution by sugar extracted spent rice biomass. *Carbohydr. Polym.* **2012**, *90*, 1314–1322. [[CrossRef](#)]
35. Mitrogiannis, D.; Markou, G.; Çelekli, A.; Bozkurt, H. Biosorption of methylene blue onto *Arthrospira platensis* biomass: Kinetic, equilibrium and thermodynamic studies. *J. Environ. Chem. Eng.* **2015**, *3*, 670–680. [[CrossRef](#)]
36. Guler, U.A.; Sarioglu, M. Single and binary biosorption of Cu(II) , Ni(II) and methylene blue by raw and pretreated *Spirogyra* sp.: Equilibrium and kinetic modeling. *J. Environ. Chem. Eng.* **2013**, *1*, 369–377. [[CrossRef](#)]
37. Daneshvar, E.; Vazirzadeh, A.; Niazi, A.; Kousha, M.; Naushad, M.; Bhatnagar, A. Desorption of Methylene blue dye from brown macroalgae: Effects of operating parameters, isotherm study and kinetic modeling. *J. Clean. Prod.* **2017**, *152*, 443–453. [[CrossRef](#)]
38. Nacéra, Y.; Aicha, B. Equilibrium and kinetic modelling of methylene blue biosorption by pretreated dead *Streptomyces rimosus*: Effect of temperature. *Chem. Eng. J.* **2006**, *119*, 121–125. [[CrossRef](#)]
39. Agarwal, S.; Tyagi, I.; Gupta, V.K.; Ghasemi, N.; Shahivand, M.; Ghasemi, M. Kinetics, equilibrium studies and thermodynamics of methylene blue adsorption on *Ephedra strobilacea* saw dust and modified using phosphoric acid and zinc chloride. *J. Mol. Liq.* **2016**, *218*, 208–218. [[CrossRef](#)]
40. Gusmão, K.A.G.; Gurgel, L.V.A.; Melo, T.M.S.; Gil, L.F. Adsorption studies of methylene blue and gentian violet on sugarcane bagasse modified with EDTA dianhydride (EDTAD) in aqueous solutions: Kinetic and equilibrium aspects. *J. Environ. Manag.* **2013**, *118*, 135–143. [[CrossRef](#)]
41. Nasuha, N.; Hameed, B.H. Adsorption of methylene blue from aqueous solution onto NaOH-modified rejected tea. *Chem. Eng. J.* **2011**, *166*, 783–786. [[CrossRef](#)]
42. Jin, Y.; Zhang, Y.; Lü, Q.; Cheng, X. Biosorption of methylene blue by chemically modified cellulose waste. *J. Wuhan Univ. Technol. Sci. Ed.* **2014**, *29*, 817–823. [[CrossRef](#)]
43. Yagub, M.T.; Sen, T.K.; Ang, M. Removal of cationic dye methylene blue (MB) from aqueous solution by ground raw and base modified pine cone powder. *Environ. Earth Sci.* **2013**, *71*, 1507–1519. [[CrossRef](#)]
44. Spagnoli, A.A.; Giannakoudakis, D.A.; Bashkova, S. Adsorption of methylene blue on cashew nut shell based carbons activated with zinc chloride: The role of surface and structural parameters. *J. Mol. Liq.* **2017**, *229*, 465–471. [[CrossRef](#)]
45. Royer, B.; Cardoso, N.F.; Lima, E.C.; Vagheti, J.C.; Simon, N.M.; Calvete, T.; Veses, R.C. Applications of Brazilian pine-fruit shell in natural and carbonized forms as adsorbents to removal of methylene blue from aqueous solutions—Kinetic and equilibrium study. *J. Hazard. Mater.* **2009**, *164*, 1213–1222. [[CrossRef](#)]
46. Pavan, F.A.; Lima, E.C.; Dias, S.L.; Mazzocato, A.C. Methylene blue biosorption from aqueous solutions by yellow passion fruit waste. *J. Hazard. Mater.* **2008**, *150*, 703–712. [[CrossRef](#)]
47. Bhagavathi Pushpa, T.; Vijayaraghavan, J.; Vijayaraghavan, K.; Jegan, J. Utilization of Effective Microorganisms based water hyacinth compost as biosorbent for the removal of basic dyes. *Desalin. Water Treat.* **2016**, *57*, 24368–24377. [[CrossRef](#)]
48. Vijayaraghavan, J.; Bhagavathi Pushpa, T.; Sardhar Basha, S.J.; Vijayaraghavan, K.; Jegan, J. Evaluation of Red Marine Alga *Kappaphycus alvarezii* as Biosorbent for Methylene Blue: Isotherm, Kinetic, and Mechanism Studies. *Sep. Sci. Technol.* **2014**, *50*, 1120–1126. [[CrossRef](#)]
49. Vijayaraghavan, J.; Bhagavathi Pushpa, T.B.; Sardhar Basha, S.J.; Jegan, J. Isotherm, kinetics and mechanistic studies of methylene blue biosorption onto red seaweed *Gracilaria corticata*. *Desalin. Water Treat.* **2015**, *57*, 13540–13548. [[CrossRef](#)]
50. Senthil Kumar, P.; Abhinaya, R.V.; Gayathri Lashmi, K.; Arthi, V.; Pavithra, R.; Sathyaselvabala, V.; Dinesh Kirupha, S.; Sivanesan, S. Adsorption of methylene blue dye from aqueous solution by agricultural waste: Equilibrium, thermodynamics, kinetics, mechanism and process design. *Colloid J.* **2011**, *73*, 651–661. [[CrossRef](#)]
51. Song, J.; Zou, W.; Bian, Y.; Su, F.; Han, R. Adsorption characteristics of methylene blue by peanut husk in batch and column modes. *Desalination* **2011**, *265*, 119–125. [[CrossRef](#)]
52. Ince, M.; Ince, O.K. An Overview of Adsorption Technique for Heavy Metal Removal from Water/Wastewater: A Critical Review. *Int. J. Pure Appl. Sci.* **2017**, *3*, 10–19. [[CrossRef](#)]
53. Oladoja, N.A.; Aboluwoye, C.O.; Oladimeji, Y.B.; Ashogbon, A.O.; Otemuyiwa, I.O. Studies on castor seed shell as a sorbent in basic dye contaminated wastewater remediation. *Desalination* **2008**, *227*, 190–203. [[CrossRef](#)]
54. Kaur, R.; Bhaskar, T. Potential of castor plant (*Ricinus communis*) for production of biofuels, chemicals, and value-added products. *Waste Biorefinery* **2020**, 269–310. [[CrossRef](#)]

55. Ladda, P.L.; Kamthane, R.B. *Ricinus communis* (castor): An overview. *Int. J. Res. Pharmacol. Pharmacother.* **2014**, *3*, 136–144.
56. Shah, S.K.; Patel, C.J.; Rathore, B.S.; Desai, A.G. Evaluation of Castor Stems Residue for Cellulose and Lignin Content. *Int. J. Agric. Environ. Biotechnol.* **2015**, *8*, 331. [[CrossRef](#)]
57. Marczenko, Z. *Spectrophotometric Determination of Elements*; Horwood: New York, NY, USA, 1975.
58. Wang, Y.H.; Liu, X.Q.; Meng, G.Y. Preparation and properties of supported 100% titania ceramic membranes. *Mater. Res. Bull.* **2008**, *43*, 1480–1491. [[CrossRef](#)]
59. Sachin, K.M.; Karpe, S.A.; Singh, M.; Bhattarai, A. Self-assembly of sodium dodecylsulfate and dodecyltrimethylammonium bromide mixed surfactants with dyes in aqueous mixtures. *R. Soc. Open Sci.* **2019**, *6*, 181979. [[CrossRef](#)]
60. Ahmed, S.; Jiang, X.; Wang, C.; Kalsoom, U.E.; Wang, B.; Khan, J.; Muhammad, Y.; Duan, Y.; Zhu, H.; Ren, X.; et al. An Insightful Picture of Nonlinear Photonics in 2D Materials and their Applications: Recent Advances and Future Prospects. *Adv. Opt. Mater.* **2021**, *9*, 2001671. [[CrossRef](#)]
61. Alagarsamy, A.; Chandrasekaran, S.; Manikandan, A. Green synthesis and characterization studies of biogenic zirconium oxide (ZrO₂) nanoparticles for adsorptive removal of methylene blue dye. *J. Mol. Struct.* **2022**, *1247*, 131275. [[CrossRef](#)]
62. Pirbazari, A.E.; Saberikhah, E.; Kozani, S.H. Fe₃O₄-wheat straw: Preparation, characterization and its application for methylene blue adsorption. *Water Resour. Ind.* **2014**, *7–8*, 23–37. [[CrossRef](#)]
63. Peres, E.C.; Slaviero, J.C.; Cunha, A.M.; Hosseini-Bandegharai, A.; Dotto, G.L. Microwave synthesis of silica nanoparticles and its application for methylene blue adsorption. *J. Environ. Chem. Eng.* **2018**, *6*, 649–659. [[CrossRef](#)]
64. Lu, K.; Wang, T.; Zhai, L.; Wu, W.; Dong, S.; Gao, S.; Mao, L. Adsorption behavior and mechanism of Fe-Mn binary oxide nanoparticles: Adsorption of methylene blue. *J. Colloid Interface Sci.* **2019**, *539*, 553–562. [[CrossRef](#)] [[PubMed](#)]
65. Sultan, M.; Jamal, Z.; Jubeen, F.; Farooq, A.; Bibi, I.; Uroos, M.; Chaudhry, H.; Alissa, S.A.; Iqbal, M. Green synthesis of biodegradable polyurethane and castor oil-based composite for benign transformation of methylene blue. *Arab. J. Chem.* **2021**, *14*, 103417. [[CrossRef](#)]
66. Zhang, Z.; Xu, L.; Liu, Y.; Feng, R.; Zou, T.; Zhang, Y.; Kang, Y.; Zhou, P. Efficient removal of methylene blue using the mesoporous activated carbon obtained from mangosteen peel wastes: Kinetic, equilibrium, and thermodynamic studies. *Microporous Mesoporous Mater.* **2021**, *315*, 110904. [[CrossRef](#)]
67. Elmorsi, T.M. Equilibrium Isotherms and Kinetic Studies of Removal of Methylene Blue Dye by Adsorption onto Miswak Leaves as a Natural Adsorbent. *J. Environ. Prot.* **2011**, *02*, 817–827. [[CrossRef](#)]
68. Sharma, K.; Sharma, S.; Sharma, V.; Mishra, P.K.; Ekielski, A.; Sharma, V.; Kumar, V. Methylene Blue Dye Adsorption from Wastewater Using Hydroxyapatite/Gold Nanocomposite: Kinetic and Thermodynamics Studies. *Nanomaterials* **2021**, *11*, 1403. [[CrossRef](#)]
69. Hashem, A.H.; Saied, E.; Hasanin, M.S. Green and ecofriendly bio-removal of methylene blue dye from aqueous solution using biologically activated banana peel waste. *Sustain. Chem. Pharm.* **2020**, *18*, 100333. [[CrossRef](#)]
70. Jawad, A.H.; Hum, N.N.M.F.; Farhan, A.M.; Mastuli, M.S. Biosorption of methylene blue dye by rice (*Oryza sativa* L.) straw: Adsorption and mechanism study. *Desalin. Water Treat.* **2020**, *190*, 322–330. [[CrossRef](#)]
71. Kavci, E.; Erkmen, J.; Bingöl, M.S. Removal of methylene blue dye from aqueous solution using citric acid modified apricot stone. *Chem. Eng. Commun.* **2021**, 1–16. [[CrossRef](#)]
72. Adegoke, K.A.; Bello, O.S. Dye sequestration using agricultural wastes as adsorbents. *Water Resour. Ind.* **2015**, *12*, 8–24. [[CrossRef](#)]
73. Miri, A.; Mahabbati, F.; Najafidoust, A.; Miri, M.J.; Sarani, M. Nickel oxide nanoparticles: Biosynthesized, characterization and photocatalytic application in degradation of methylene blue dye. *Inorg. Nano-Metal Chem.* **2020**, *52*, 122–131. [[CrossRef](#)]
74. Dhananasekaran, S.; Palanivel, R.; Pappu, S. Adsorption of Methylene Blue, Bromophenol Blue, and Coomassie Brilliant Blue by α -chitin nanoparticles. *J. Adv. Res.* **2016**, *7*, 113–124. [[CrossRef](#)] [[PubMed](#)]
75. Awad, A.M.; Jalab, R.; Benamor, A.; Nasser, M.S.; Ba-Abbad, M.M.; El-Naas, M.; Mohammad, A.W. Adsorption of organic pollutants by nanomaterial-based adsorbents: An overview. *J. Mol. Liq.* **2020**, *301*, 112335. [[CrossRef](#)]
76. Ahmad, K.; Shah, H.R.; Ahmad, M.; Ahmed, M.; Naseem, K.; Riaz, N.; Muhammad, A.; Ayub, A.; Ahmad, M.; Ahmad, Z.; et al. Comparative Study Between Two Zeolitic Imidazolate Frameworks as Adsorbents for Removal of Organoarsenic, As(III) and As(V) Species from Water. *Braz. J. Anal. Chem.* **2022**, *9*, 78–97. [[CrossRef](#)]
77. Ahmad, K.; Shah, H.U.; Ashfaq, A.; Ashfaq, M.; Kashif, M.; Naseem, H.A.; Aziz, T.; Parveen, S.; Nazir, I. Synthesis of New Series of Phenyl diazene Based Metal Complexes for Designing Most Active Antibacterial and Antifungal Agents. *J. Chem. Soc. Pak.* **2021**, *43*, 578. [[CrossRef](#)]
78. Shah, H.U.R.; Ahmad, K.; Naseem, H.A.; Parveen, S.; Ashfaq, M.; Aziz, T.; Shaheen, S.; Babras, A.; Shahzad, A. Synthetic routes of azo derivatives: A brief overview. *J. Mol. Struct.* **2021**, *1244*, 131181. [[CrossRef](#)]
79. Suhaimi, N.; Kooh, M.R.; Lim, C.M.; Chou Chao, C.-T.; Chou Chau, Y.F.; Mahadi, A.H.; Chiang, H.P.; Hassan, N.H.; Thotagamuge, R. The Use of Gigantochloa Bamboo-Derived Biochar for the Removal of Methylene Blue from Aqueous Solution. *Adsorpt. Sci. Technol.* **2022**, *2022*, 8245797. [[CrossRef](#)]
80. Kooh, M.R.R.; Thotagamuge, R.; Chou Chau, Y.-F.; Mahadi, A.H.; Lim, C.M. Machine learning approaches to predict adsorption capacity of *Azolla pinnata* in the removal of methylene blue. *J. Taiwan Inst. Chem. Eng.* **2022**, *132*, 104134. [[CrossRef](#)]